



Article

Hydrodynamic Analysis of a Multi-Pile-Supported Offshore Wind Turbine Integrated with an Aquaculture Cage

Zhisheng Tu ^{1,2} , Cailiang Zhang ^{1,2,3}, Hanqiu Liu ^{1,2} and Ronghua Zhu ^{1,2,3,*} 

¹ Ocean College, Zhejiang University, Zhoushan 316021, China; 12234011@zju.edu.cn (Z.T.); 12034092@zju.edu.cn (C.Z.); liuhanqiu@zju.edu.cn (H.L.)

² Yangjiang Offshore Wind Power Laboratory, Yangjiang 529500, China

³ Hainan Institute, Zhejiang University, Sanya 572025, China

* Correspondence: zhu.richard@zju.edu.cn

Abstract: The integrated development of offshore wind power and marine aquaculture is becoming increasingly important. However, the impact mechanism of integrating a net cage on the dynamic characteristics of offshore wind turbines remains unclear. This paper presents a design scheme for a multi-pile-supported offshore wind turbine integrated with an aquaculture net cage and conducts a preliminary theoretical analysis of the influence of an additional net cage on the wind turbine. The analysis reveals that the primary effect is an increase in hydrodynamic loads on the wind turbine foundation, while the structural frequency of the wind turbine remains largely unaffected. Furthermore, computational fluid dynamics (CFD) numerical models, whose accuracy is verified by physical experiments, are utilized to compare the hydrodynamic characteristics of the offshore wind turbine foundation with and without the net cage, considering different net solidities. The simulations identify significant changes in the flow field surrounding the foundation due to the presence of the net cage, resulting in a considerable increase in the overall hydrodynamic load on the foundation. Moreover, the mutual interference between the netting and the foundation amplifies their respective hydrodynamic loads and concentrates these loads at the upstream section of the structure. The maximum increase in hydrodynamic load for a single pile reaches 6.32 times its original value, posing significant risks to the structure. Finally, a preliminary feasibility analysis of the scheme was conducted. The results presented in this article can serve as a theoretical basis for the design of such innovative structures.



Citation: Tu, Z.; Zhang, C.; Liu, H.; Zhu, R. Hydrodynamic Analysis of a Multi-Pile-Supported Offshore Wind Turbine Integrated with an Aquaculture Cage. *J. Mar. Sci. Eng.* **2023**, *11*, 1830. <https://doi.org/10.3390/jmse11091830>

Academic Editor: Kamal Djidjeli

Received: 16 August 2023

Revised: 13 September 2023

Accepted: 15 September 2023

Published: 20 September 2023



Copyright: © 2023 by the authors. Licensee MDPI, Basel, Switzerland. This article is an open access article distributed under the terms and conditions of the Creative Commons Attribution (CC BY) license (<https://creativecommons.org/licenses/by/4.0/>).

Keywords: offshore wind turbine; aquaculture net cage; structure integration; hydrodynamic characteristics

1. Introduction

Offshore wind power is a highly promising and significant renewable energy source in the quest to achieve carbon neutrality targets. It has witnessed rapid global development in recent years. According to the Global Wind Energy Council (GWEC) report [1], 8.8 GW of new offshore wind was fed into the grid last year. By the end of 2022, the cumulative installed capacity of offshore wind power worldwide reached 64.3 GW, with a compound annual growth rate of +19.2% over the past five years. Moreover, the GWEC Market Intelligence predicts that the global offshore wind market will continue to grow at an accelerated pace. Currently, the fixed offshore wind turbine is the main form of offshore wind turbines globally, with monopile foundations and jacket foundations being the most common foundation types [2,3]. Fixed wind turbines obtain soil bearing capacity by embedding the foundation structure into the seabed to resist the wind, wave, and current loads on the wind turbines [4]. In recent decades, many scholars have conducted research on the dynamic characteristics of offshore wind turbines under the effects of wind, waves, currents, earthquakes, and other loads [5–7], resulting in a relatively mature research foundation in this field. Based on this, organizations such as Det Norske Veritas (DNV),

the American Bureau of Shipping (ABS), the American Petroleum Institute (API), and the American Society of Civil Engineers (ASCE) have developed relevant standards for the calculation of dynamic responses of offshore wind turbines, which detail how to conduct offshore wind turbine design work [8,9]. However, offshore wind turbines require substantial investment, and the cost of electricity generation is higher compared to other traditional power generation methods. The integration of offshore wind power with other offshore industries is considered an effective strategy for cost reduction [10].

Marine aquaculture also plays a crucial role in the ocean economy, utilizing seawater resources below the sea level to provide high-quality marine food and supplement protein, contributing to significant development value [11]. Over the past few decades, global marine aquaculture has experienced rapid growth, transitioning from a relatively minor role to a mainstream component of the global food system [12]. According to the statistics from the Food and Agriculture Organization of the United Nations (FAO), global aquaculture production reached 87.5 million tons in 2020, with marine aquaculture production accounting for 33.1 million tons, representing a growth rate of 23.5% over the past decade [13]. Compared to other forms of meat production, fish and seafood production require less land and fresh water, while generating fewer greenhouse gases. This makes aquaculture environmentally friendly, aligning with the goals of achieving carbon neutrality [14,15]. Additionally, although the ocean covers 71% of the Earth's surface, it only provides 13% of fishery value [12], indicating that marine aquaculture has great potential for development.

Currently, marine aquaculture facilities are primarily located in shallow waters near coastal areas. However, these facilities face challenges, such as poor resistance to wind and waves, resource overexploitation in shallow waters, and degradation of the aquaculture environment. As a response, the development of deep-sea aquaculture facilities has gained prominence, with over 20 countries worldwide engaging in research and development efforts in this area [16]. The most representative of these is the large-scale deep-sea aquaculture cage, which has strong resistance to wind and waves, a large aquaculture space, and various environmental advantages, such as low pollution and eutrophication, relatively stable temperatures, and sufficient water exchange inside and outside the cage [17]. However, the design complexity associated with large-scale deep-sea cages is considerable, as exemplified by the world's first large-scale deep-sea cage, known as Ocean Farm 1 [18]. In addition, a large-scale pile-net enclosure aquaculture facility has emerged in recent years, with advantages such as a large aquaculture area, large fish activity space, closer-to-natural aquaculture environment, and improved quality of aquaculture fish [19].

Large-scale aquaculture facilities encounter significant wave and current loads during their operation, necessitating thorough structural hydrodynamic analysis. Many researchers have delved into related studies, with a particular focus on the challenge posed by the flexible netting component in the structural design. Despite the development of the aquaculture net cage industry over several decades, empirical methods still dominate the design practices within the industry [20]. The hydrodynamic behavior of flexible netting can be divided into two key aspects: the hydrodynamic characteristics of the netting itself and the interaction between the netting and the surrounding flow. Presently, researchers primarily explore netting behavior using physical model experiments and numerical simulations. Xu et al. [21] provided a summary of the research concerning netting simulation methods, which can be categorized into three main approaches: the finite element method, computational fluid dynamics method, and fluid–structure interaction method.

Many scholars have focused on the hydrodynamic characteristics of the netting itself and have achieved significant research through physical model experiments and finite element numerical simulations. For example, based on physical model experiments, Løland [22], Tsukrov [23], Tang [24], Lader [25], etc., established two hydrodynamic calculation models of netting, namely the Morison model and the Screen model, and proposed corresponding empirical formulas. Based on these empirical formulas, scholars such as Moe-Føre [26], Li [27], Shainee [28], Faltinsen [29], Takagi [30], etc., used beam elements, truss elements, and concentrated mass-spring models to construct numerical models of

net cages, forming various hydrodynamic characteristic numerical analysis codes, such as Aqua-FE, AquaSim, DUT-FlexSim, NaLA, and MPSL, which can be used to accurately evaluate the hydrodynamic load and deformation of net cages [31]. However, using the finite element method to establish numerical models of the netting cannot, on its own, simulate the interference of net cages and the surrounding flow. Currently, we can use empirical formulas to only roughly evaluate the mutual interference between net cages, such as the upstream net cages' wake effect on the downstream net cage.

The study of the flow field around the netting primarily relies on the CFD method, apart from model experiments. Authors such as Zhao [32,33] and Bui [34] used the porous media model to simulate netting and conducted research on the characteristics of the flow field around netting. However, the porous media model has its limitations; it is considered a substitute, sharing similar physical properties as the original interaction process. This, however, does not imply any physical connection [35]; it only approximates the drag reduction effect of the netting and cannot consider the deformation of the netting itself [21].

Therefore, researchers have also put forth the fluid–structure interaction method for netting simulation to jointly analyze the hydrodynamic characteristics of the netting and the surrounding flow. However, due to the flexibility of the netting and the small mesh scale, establishing a numerical model that accurately represents the netting is challenging, and this area of research is still in its early stages. Bi [36] and Chen [37] respectively developed a fluid–structure coupling net cage model that combines a porous medium model and a concentrated mass model to represent the deformation of the net cage. Cheng et al. [38] proposed a fluid–structure coupling algorithm based on open FOAM and Code-Aster, two types of open-source software, using an improved dynamic porous media model and a screen model to simplify the numerical model. Yao et al. [39] established a coupling algorithm combining the finite volume method and mass-spring model, and preliminarily analyzed the hydrodynamic characteristics of the net cage under stable flow. The research available on the fluid–structure coupling method for netting is limited, and accurately evaluating the hydrodynamic behavior and surrounding flow fields of the netting remains a significant challenge within the industry [20].

Both offshore wind turbine and marine aquaculture industries are significant users of sea space. As these industries continue to grow on a large scale, conflicts over the utilization of sea space have emerged [40]. The integration of the two can effectively solve many problems faced by both industries and improve the level of marine development; thus, this area has become a research hotspot. Scholars in these industries have conducted relevant research and demonstrated the feasibility of the integrated development of the two industries [41–43].

The integrated development models for these two industries are categorized into two types. The first type involves utilizing the vacant areas within offshore wind farms to deploy aquaculture facilities. The second type involves installing aquaculture cages directly onto the foundations of the wind turbines, utilizing the foundations for support. The latter approach is a form of structural integration, which can lead to greater cost reductions but also presents greater design challenges and multiple problems to solve. Some scholars have proposed new foundations for integrating cages based on different types of offshore wind turbine foundations. For example, Li et al. [44] based their study on the jacket foundation, Zhai et al. [45] based their study on the barge foundation, and Zhang et al. [46] based their study on the semi-submersible foundation. They independently proposed an offshore wind turbine foundation integrated with a net cage and established numerical models to conduct dynamic analysis of the whole structure and evaluate the impact of additional netting on the structure. In addition, Lei et al. [47] also proposed a new type of integrated structure by installing a wind turbine on a large deep-sea cage.

However, most of the research above adopts numerical simulation methods, which equate the netting to a rigid rod and evaluate the hydrodynamic loads of the netting using the Morison formula, which is widely used in the field of offshore engineering due to its simplicity and convenience in calculations. However, it cannot evaluate the mutual flow

field interference between the netting and the foundation or be used for the surrounding flow field of the foundation for it does not establish a numerical model of flow. According to relevant experimental studies on large deep-sea cages, the existence of flexible netting will significantly change the flow field around the structure and have a significant impact on the hydrodynamic characteristics of the structure [48]. Therefore, it is crucial to consider the mutual flow field interference between the netting and the foundation. Overall, the current research on the integrated structure of offshore wind turbines and aquaculture cages remains limited, particularly concerning the mechanism of the additional netting's impact on offshore wind turbines. The exploration of hydrodynamic load variations resulting from the mutual flow field interference between the netting and the foundation has not been thoroughly investigated. Consequently, the current knowledge is inadequate to meet the requirements for designing such engineering structures, and further research is necessary.

Based on these considerations, this paper focuses on meeting the requirements of an actual engineering project by investigating the integration of a fixed multi-pile-support offshore wind turbine with an aquaculture net cage. The multi-pile-supported offshore wind turbines were initially applied in waters with a depth of less than 20 m in China and will have some applications in the emerging Southeast Asian offshore wind market. This type of foundation is suitable for relatively shallow waters and has good feasibility in the integrated development of offshore wind turbines and marine aquaculture. It has broad application prospects. However, there is currently no research specifically focusing on the combination of such offshore wind turbines with marine aquaculture cages.

The primary objective of this paper is to propose a new design scheme for their integration. Applying principles from structural dynamics and wind turbine design theory, the study conducts a preliminary analysis of the impact of additional netting on the offshore wind turbines. The findings reveal that the main effect of the additional netting is an increase in wave and current loads on the wind turbine foundation, while having minimal impact on the structural frequency. To further comprehend these additional hydrodynamic loads and examine the interaction between the netting and the foundation, Computational Fluid Dynamics (CFD) simulations, whose accuracy is verified by physical model experiments, are employed to analyze and compare the hydrodynamic characteristics of the offshore wind turbine foundation before and after the addition of the netting, for the first time, considering different net solidities. By doing this, the effects on the surrounding flow field and the hydrodynamic loads of the foundation, due to the presence of the net cage, can be analyzed. Finally, a preliminary feasibility analysis of the scheme was conducted, considering the economic viability and advantages. The results presented in this article can serve as a theoretical basis for the design of such innovative structures.

The remainder of this paper is organized as follows: Section 2 introduces the structure design scheme and theoretical methods used in this research. Section 3 presents a preliminary theoretical analysis of the structure. In Section 4, the numerical model and model validation are reported. Section 5 presents the results and discussion. The conclusions are presented in Section 6. Finally, Section 7 presents future work.

2. Structure Design Scheme and Theoretical Methods

2.1. Structure Design Scheme

Fixed foundations for offshore wind turbines encompass various forms, including mono-pile foundations, multi-pile-support foundations, and jacket foundations. Among these, the multi-pile-support foundation and jacket foundation create an interior space within the piles, which can be enclosed by connecting them with net panels, thus forming an aquaculture net cage. This approach eliminates the need for the conventional framework structure and mooring system typically required by aquaculture net cages. It presents a straightforward, cost-effective, and efficient method for constructing net cages, enabling the integration of offshore wind turbines and aquaculture cages. Thus, a novel fusion structure has emerged.

In the discussed offshore wind farm project, the multi-pile-support foundation is adopted. Figure 1 showcases the model of the offshore wind turbine with an aquaculture net cage, while Figure 2 illustrates the design drawing and model of the offshore wind turbine foundation with and without the net cage. The multi-pile-support foundation comprises steel pipe piles and a concrete platform. The concrete platform has a diameter of 14.2 m, with eight steel pipe piles evenly distributed along its circumference. Each steel pipe pile has an outer diameter of 1.6 m and a spatial slope of 5:1. The enclosed space formed by the eight steel pipe piles serves as an ideal environment for fish farming. By incorporating net panels between the piles, it transforms into an offshore wind turbine foundation integrated with an aquaculture net cage (WT-NC), as demonstrated in Figure 2. Regarding the net cage layout elevation, the upper end of the net cage is raised 3 m above the extreme high tide level to prevent fish from escaping, while the lower end is elevated 2 m above the highest seabed level to ensure that the net cage does not make contact with the seabed. These measures maintain the integrity and functionality of the net cage. The specific design parameters of the offshore wind turbine foundation with the net cage are shown in Table 1 below.

Table 1. Main parameters of the foundation with net cage.

Component	Parameters	Value
Foundation	Diameter of pile (m)	1.6
	Slope of pile	5:1
	Diameter of platform (m)	14.2
	Diameter of pile top circle (m)	10
Netting	Size of mesh (mm)	40
	Diameter of net wire (mm)	4
	Net panel size (L1 × L2 × H) (m)	2.96 × 5.74 × 18.51
	Area of net panel (m ²)	80.52
	Net solidity	0.2
	Net material	Ultra-High Molecular Weight Polyethylene Fiber
	Net density (g/cm ³)	0.97–0.98

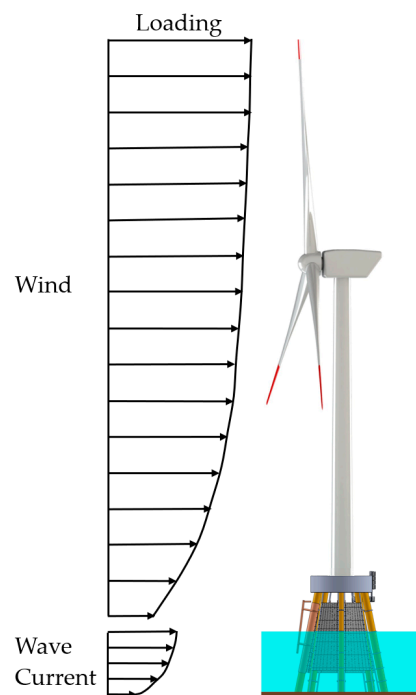


Figure 1. Model of the offshore wind turbine with an aquaculture net cage.

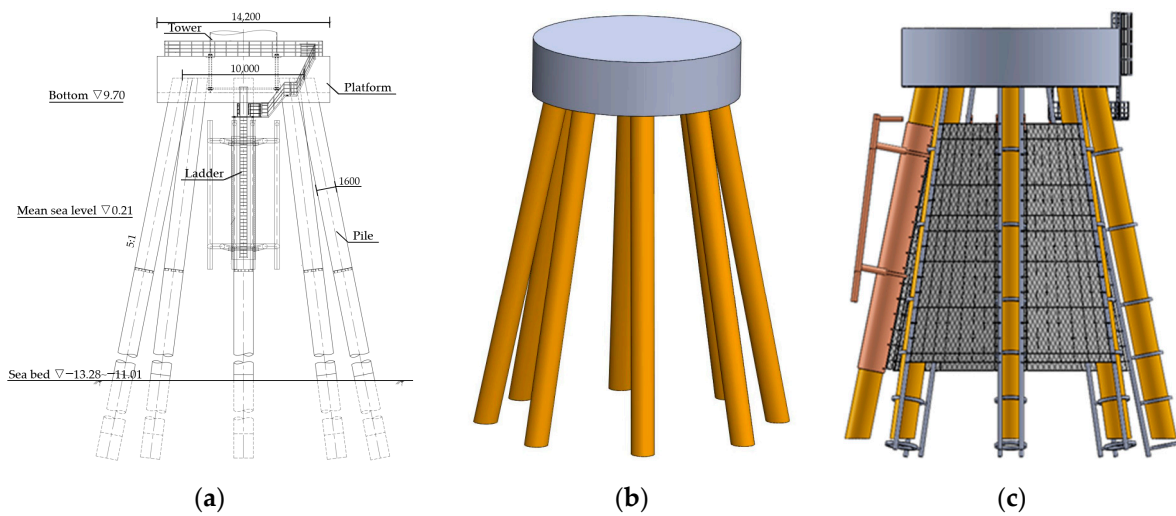


Figure 2. Design drawing and model of the foundation. (a) Design drawing of the multi-pile-support foundation; (b) model of the multi-pile-support foundation; (c) model of the multi-pile-support foundation with an aquaculture net cage.

2.2. Theoretical Methods

Offshore wind turbines are towering structures located in the ocean, designed to withstand various environmental loads, such as wind, waves, and currents, during their operation. The dynamic response of these structures is complex and requires structural dynamic analysis. Additionally, this article utilizes the CFD method to analyze the hydrodynamic loads acting on the offshore wind turbine foundation integrated with an aquaculture cage. The theoretical methods employed in this study are described below.

2.2.1. Vibration Equation of the Structure

The general form of the structural vibration equation for a multi-degree-of-freedom system is as follows:

$$M\ddot{Y}(t) + C\dot{Y}(t) + KY(t) = P(t) \tag{1}$$

where M is the mass matrix of the system, C is the damping matrix, K is the stiffness matrix, $Y(t)$ is the displacement of the system, and $P(t)$ is the disturbance force of the system.

2.2.2. Governing Equations of Fluid

This article employs the CFD method to analyze structural hydrodynamic loads and considers the incompressible flow, using the Realizable $k - \epsilon$ turbulence model [49]. The main equations involved are as follows:

Continuity equation:

$$\frac{\partial \rho}{\partial t} + \frac{\partial(\rho u_i)}{\partial x_i} = 0 \tag{2}$$

Momentum equation:

$$\frac{\partial \rho u_i}{\partial t} + \frac{\partial(\rho u_i u_j)}{\partial x_j} = -\frac{\partial P}{\partial x_i} + \rho g_i + \frac{\partial}{\partial x_i}(\mu + \mu_t)\left(\frac{\partial u_i}{\partial x_j} + \frac{\partial u_j}{\partial x_i}\right) \tag{3}$$

$$P = p + (2/3)\rho k \tag{4}$$

where t represents time, ρ is the density of the fluid, μ is the dynamic viscosity of the fluid, μ_t is the eddy viscosity, p is the pressure, k is the turbulent kinetic energy, u_i and u_j are the time-mean velocity components, g_i is the gravitational acceleration, and $i, j = 1, 2, 3$ represent the coordinate components.

The governing equations are discretized by the finite volume method. After the calculation domain is discretized into unit bodies, each physical quantity is discretely distributed on the center of each unit body. Then, the integral equation on the unit body is transformed into an algebraic equation expressed by the quantity on the center of the unit body. Finally, the numerical solution can be obtained by solving the algebraic equations. The SIMPLEC algorithm is selected for pressure–velocity coupling. The second-order upwind scheme is adopted for the discretization of pressure, momentum, turbulent kinetic energy, and dissipation rate.

For the realizable $k - \varepsilon$ turbulence model, the main equations involved are as follows:
 k equation:

$$\frac{\partial(\rho k)}{\partial t} + \frac{\partial(\rho k u_j)}{\partial x_j} = \frac{\partial}{\partial x_j} \left[\left(\mu + \frac{\mu_t}{\sigma_k} \right) \frac{\partial k}{\partial x_j} \right] + G_k + G_b - \rho \varepsilon - Y_M + S_k \tag{5}$$

ε equation:

$$\frac{\partial(\rho \varepsilon)}{\partial t} + \frac{\partial(\rho \varepsilon u_j)}{\partial x_j} = \frac{\partial}{\partial x_j} \left[\left(\mu + \frac{\mu_t}{\sigma_\varepsilon} \right) \frac{\partial \varepsilon}{\partial x_j} \right] + \rho C_1 S \varepsilon - \rho C_2 \frac{\varepsilon^2}{k + \sqrt{v \varepsilon}} + C_{1\varepsilon} \frac{\varepsilon}{k} C_{3\varepsilon} G_b + S_\varepsilon \tag{6}$$

$$C_1 = \max \left[0.43, \frac{\eta}{\eta + 5} \right], \eta = S \frac{k}{\varepsilon}, S = \sqrt{2 S_{ij} S_{ij}}, S_{ij} = \frac{1}{2} \left(\frac{\partial u_i}{\partial x_j} + \frac{\partial u_j}{\partial x_i} \right) \tag{7}$$

where G_k is the turbulent kinetic energy generated by the average velocity gradient, G_b is the turbulent kinetic energy generated by buoyancy, Y_M is the overall dissipation rate of fluctuating diffusion in compressible turbulence, C_2 and $C_{1\varepsilon}$ are constants, S is a strain modulus, σ_k and σ_ε are the turbulent Prandtl numbers for k and ε , S_k and S_ε are the user-defined source terms. In this paper, the fluid is incompressible and the temperature is not considered, yielding $G_b = 0$, $Y_M = 0$, $S_k = 0$, and $S_\varepsilon = 0$. $C_{1\varepsilon} = 1.44$ and $C_2 = 1.9$ are constants.

2.2.3. Hydrodynamic Empirical Equation of the Structure

For small-scale ocean structures, the calculation of wave and current loads can be based on the Morison equation:

$$F = 0.5 \rho C_D A v |v| + \rho C_M V \dot{v} \tag{8}$$

where F is the structural hydrodynamic load; C_D is the drag coefficient; C_M is the inertia coefficient; ρ is the density of the fluid; v is the velocity of the fluid particle; \dot{v} is the acceleration of the fluid particle; A is the projected area of the structure; and V is the volume of the structure.

3. Structure Theoretical Analysis

Based on the theory of structural dynamics, a preliminary analysis is conducted on the dynamic characteristics of the WT–NC proposed in this article. Since the offshore wind turbine is the main focus, it is crucial to ensure the turbine’s safety during the design of the WT–NC. Therefore, an evaluation is carried out to assess the impact of the additional netting on the offshore wind turbine from a wind turbine design perspective.

The offshore wind turbine is a towering and flexible marine structure primarily exposed to wind and wave loads. The coupling effect of wind and waves leads to significant dynamic responses in the offshore wind turbine. According to the relevant design specifications for offshore wind turbines [50], the structural design mainly encompasses three aspects: structural frequency, load-bearing capacity, and strength and displacement. The subsequent analysis examines the impact of the additional netting on the wind turbine separately in terms of these three aspects.

3.1. Structural Frequency

From the structural vibration equation, it is evident that the structural frequency depends on the distribution of structural mass, stiffness, and damping.

Firstly, let us discuss the distribution of structural mass. For the multi-pile-support foundation integrated with a net cage in this article, the netting includes bottom and side net panels. The total mass of the netting can be calculated from its parameters to be 654.43 kg, with the density of 0.97–0.98 g/cm³, which is less than 1 ton. However, according to the engineering quantity statistics of the foundation shown in Table 2, the foundation where the netting is located is constructed with filled core concrete steel piles, and its mass is approximately 692.7 tons. The wind turbine foundation includes steel pipe piles, filled core concrete, a concrete platform, and associated components, with a total mass of 2884.12 tons. When considering the upper tower and the wind turbine itself, the overall mass of the wind turbine structure exceeds 3000 tons, while the mass of the netting accounts for less than 0.03%. Therefore, the impact of the additional netting on the distribution of the wind turbine’s structural mass is negligible and can be ignored.

Table 2. Engineering quantity statistics of the foundation.

Parameters	Value
Piles (t)	893.58
Concrete of platform (m ³)	622.04
Core filled concrete (m ³)	155.51
Rebar of platform (t)	89.42
Barge bumper and ladder (t)	20
Other components (t)	15
Density of concrete (t/m ³)	2.4

Regarding the stiffness distribution of the offshore wind turbine, it resembles a tower-
ing structure, similar to a cantilever beam, where the overall stiffness primarily comes from the piles embedded in the seabed. The netting, being a flexible structure connected between the piles, does not contribute to enhancing the foundation’s ability to resist deformation caused by external loads. Therefore, adding the netting will not increase the structural stiffness of the offshore wind turbine.

Concerning the damping distribution of the offshore wind turbine, structural damping refers to the resistance encountered by the internal structure and external air and seawater when the structure vibrates. In the case of external air and seawater damping, the forces act reciprocally, and the external resistance to structural vibration follows the same calculation format as the hydrodynamic load experienced by the fixed structure. Consequently, the structural vibration damping can be evaluated using the Morison equation. Given the small diameter of the netting wire, typically ranging from 3 to 5 mm, the drag force significantly surpasses the inertial force in opposing the netting’s vibration. Hence, the primary resistance affecting the netting is the drag force.

Considering the structural self-vibration of the offshore wind turbine, the vibration of the netting originates from the wind turbine foundation. During the operation of an offshore wind turbine, the horizontal displacement at the foundation is minimal, and design standards dictate that the cumulative rotation angle of the wind turbine at the seabed surface should not exceed 0.25 degrees or 0.436% [50]. Typically, the horizontal displacement of the foundation is in the order of centimeters. In the case of the multi-pile-supported foundation described in this article, it exhibits a higher lateral stiffness. After calculation, it is determined that the maximum horizontal displacement of the foundation below the sea level is less than 4 cm, while the span of the net panel ranges from 2.96 to 5.74 m.

The net panel is a flexible structure, and the slight vibration of the foundation is transformed into waves propagating along the span of the net panel. However, due to the relatively small wavelength compared to the span of the net, multiple waves are generated

along the net panel's span rather than driving the entire net panel to vibrate in a single direction. As adjacent waves on the net panel are oriented in opposite directions, the resistance to net panel vibration cancels out, resulting in a minimal resistance force that cannot be transferred to the foundation. Furthermore, the netting only occupies a small portion of the wind turbine. When the structure vibrates in any direction, the netting's proportion of the overall projected area of the offshore wind turbine is small. Moreover, the vibrations of the net panels under the influence of waves manifest as loads rather than damping. Therefore, the additional netting has little effect on the overall structure damping distribution of the offshore wind turbine.

Overall, the additional netting has a minimal impact on the mass distribution, damping distribution, and stiffness of the offshore wind turbine structure. Therefore, the effect of the additional netting on the structural frequency of the offshore wind turbine can be ignored.

3.2. Structural Load-Bearing Capacity

When designing the load-bearing capacity of an offshore wind turbine, it is necessary to consider two aspects: load and resistance. The term "load" refers to the actual forces and loads that the offshore wind turbine experiences, while "resistance" pertains to the designed load-bearing capacity of the turbine, indicating its ability to withstand external forces. If the actual loads imposed on the offshore wind turbine are lower than its design load-bearing capacity, it signifies that the turbine's load-bearing capacity meets the design requirements.

During operation, offshore wind turbines endure primarily horizontal loads, including wind turbine load, upper structure wind load, and foundation wave/current loads. The overall structure of an offshore wind turbine resembles that of a cantilever beam. Consequently, the aforementioned horizontal loads subject the turbine structure to horizontal shear forces and the resultant bending moments.

Upon the addition of netting, the wave and current loads on the foundation experience an increase. Both the foundation and netting fulfill the conditions for implementing the Morison formula. Considering the projected area of the structure, the projected area of the netting wires is of a similar magnitude to that of the foundation. Hence, the wave and current loads on the netting cannot be disregarded. Additionally, the netting connects all the piles together, creating a net cage that enhances the mutual interference between the structures and further amplifies the total wave and current loads on the foundation.

Wave and current loads constitute significant components of offshore wind turbine loads, and the presence of netting can double or even triple the wave and current loads on the foundation. This warrants attention and careful consideration. Meanwhile, the ability of offshore wind turbines to withstand external loads primarily relies on the piles embedded in the seabed, and the presence of netting does not increase the wind turbine's design load-bearing capacity. Therefore, the presence of netting presents a formidable challenge to the load-bearing capacity of the offshore wind turbine. Accurate evaluation of the additional load imposed by the netting is crucial for offshore wind turbine design.

3.3. Structural Strength and Displacement

As mentioned above, the overall structure of an offshore wind turbine resembles that of a cantilever beam. During operation, it primarily experiences horizontal loads and the resultant bending moments. The stress on the structure increases closer to the seabed. As mentioned previously, the installation of additional netting can potentially double or even further amplify the wave and current loads on the foundation. This, in turn, increases the stress and displacement of the foundation, posing a higher risk of structural failure. Therefore, conducting an accurate assessment of these loads is essential.

Furthermore, since both ends of the net panels are fixed to the piles using ropes, the tension in the net panels aligns with the direction of the ropes. When the net panels are under load, the tension in the ropes generates two components: one that balances the loads from the waves and currents in the direction of their motion, and another perpendicular component that is dependent on the deviation angle of the ropes' fixing points on the net

panels. Designing the net panels requires controlling their deformation, particularly the deflection angle of the ropes. When the waves are perpendicular to the net panel, the perpendicular component of the tension is generally several times larger than the wave loads acting on the net panels. The presence of this component further increases the stress on the foundation. Consequently, the design process of the net panels also necessitates calculating their deformation to accurately assess the tension in the ropes.

3.4. Brief Summary

Based on the theory of structural dynamics, this section aims to provide a preliminary analysis of the impact of the additional netting on offshore wind turbines from the perspective of offshore wind turbine design. The analysis reveals that the primary effect of the additional netting on offshore wind turbines is the introduction of extra wave and current loads on the turbine foundation. These additional loads have the potential to double or even triple the loads on the foundation, thereby posing significant challenges to the structural load-bearing capacity, strength, and displacement of the foundation. However, the impact on the structural frequency of the offshore wind turbine can be negligible.

4. Numerical Model

To further analyze the mechanism of the impact of the additional netting on wave and current loads on the foundation, it is necessary to conduct an analysis of the flow field around the foundation and evaluate the interaction between the netting and the foundation. This section centers on the hydrodynamic characteristics of the offshore wind turbine foundation integrated with a net cage and establishes a numerical model utilizing the CFD method. The study examines the alterations in hydrodynamic loads on the foundation before and after the inclusion of the netting, subsequently evaluating the effects of the additional netting on the hydrodynamic loads.

4.1. Netting Model

The netting wire can be treated as slender rods that satisfy the requirements for applying the Morison equation [51]. Based on the Morison equation, the wave load on the netting is predominantly governed by drag force rather than inertia force, owing to the small diameter of the netting wire, typically ranging from 3 to 5 mm. Similarly, the current load on the netting also manifests as a drag force, computed using the same formula as the drag force for wave load, as both are dependent on the velocity of water particles. Under extreme conditions, the maximum wave and current loads occur when the velocities of water particles in both waves and currents align parallel to the horizontal direction. By conducting a preliminary static analysis, it is observed that the effect of waves on the structure is similar to that of currents. Therefore, the analysis of hydrodynamic loads on the structure focuses on considering the influence of currents alone instead of combining the effects of waves and currents.

In the proposed design of the WT-NC, the netting consists of eight net panels that are securely attached to a rigid frame composed of steel pipe piles. The net panels span a range of 2.96–5.74 m and are pre-tensioned during engineering installation to minimize deformation. In comparison to traditional flexible collar fish cages, the net panel deformation in this design is negligible and can be disregarded [52]. Moreover, under steady currents, the net panel deformation tends to stabilize, resulting in minimal fluid–structure interaction. Although neglecting the net panel deformation may lead to an overestimation of the hydrodynamic loads, conducting preliminary analysis of the netting based on this assumption still holds research significance [53]. Additionally, considering the complexities involved in accounting for netting deformation, it is often excluded in similar studies. Therefore, for the purpose of conducting preliminary analysis of the hydrodynamic loads on the WT-NC, the numerical model treats the netting as a rigid body and disregards its deformation.

Given the small dimensions of the mesh and wire diameter in the netting, typically measured in millimeters, the number of mesh segments in a net cage is usually very high. If we were to develop a numerical model based on the actual size of the net cage for hydrodynamic calculations, it would result in tremendous computational requirements, making it impractical. Hence, a method of mesh grouping was devised to establish a numerical model for the netting. This method involves grouping multiple small mesh segments into a single virtual large mesh, ensuring computational feasibility [54,55]. Since this article considers the netting as a fixed rigid structure, maintaining consistency between pre- and post-equivalent hydrodynamic loads is essential. To achieve this, the projected area of the wires before and after equivalence must remain constant. Based on this principle, four different net panel models were established: an actual-size model, a 2×2 mesh group model, a 4×4 mesh group model, and an 8×8 mesh group model, as shown in Figure 3. Numerical simulations were then conducted to validate the accuracy and effectiveness of the mesh grouping method employed in this study.

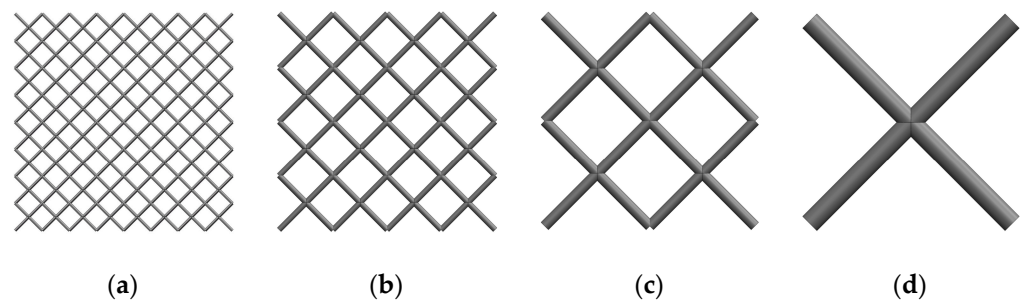


Figure 3. Mesh group models: (a) actual-size model; (b) 2×2 mesh group model; (c) 4×4 mesh group model; (d) 8×8 mesh group model.

The hydrodynamic analysis was performed on the aforementioned mesh group models of the net panels, and the hydrodynamic load acting on them was extracted in the direction of flow at a velocity of 2 m/s. The obtained results are presented in Table 3, indicating that the hydrodynamic loads on the net panel models approximate 70 N, with a maximum average deviation of 7.21%. Taking into consideration the presence of vortices and potential calculation errors, it can be concluded that the utilization of the mesh grouping method for equivalent calculation of the netting is indeed feasible. Thus, based on this finding, along with the consideration of the actual size of the netting in the WT-NC and the computational complexity involved, a numerical model for the netting is established using a 32×32 grouping mesh.

Table 3. Mesh grouping verification.

Model	Load/N
Actual-size model	67.56
2×2 mesh group model	73.17
4×4 mesh group model	71.48
8×8 mesh group model	65.91

4.2. WT-NC Model

The offshore wind turbine multi-pile-support foundation consists of eight steel pipe piles, with the netting being fixed onto them. In order to simplify the numerical model of the WT-NC, the structural connections between the netting and the piles are disregarded. Furthermore, the hydrodynamic load exerted on the bottom net panel of the net cage is negligible, and therefore, it is also excluded from the analysis. Taking into account various net solidities, the WT-NC models are depicted in Figure 4.

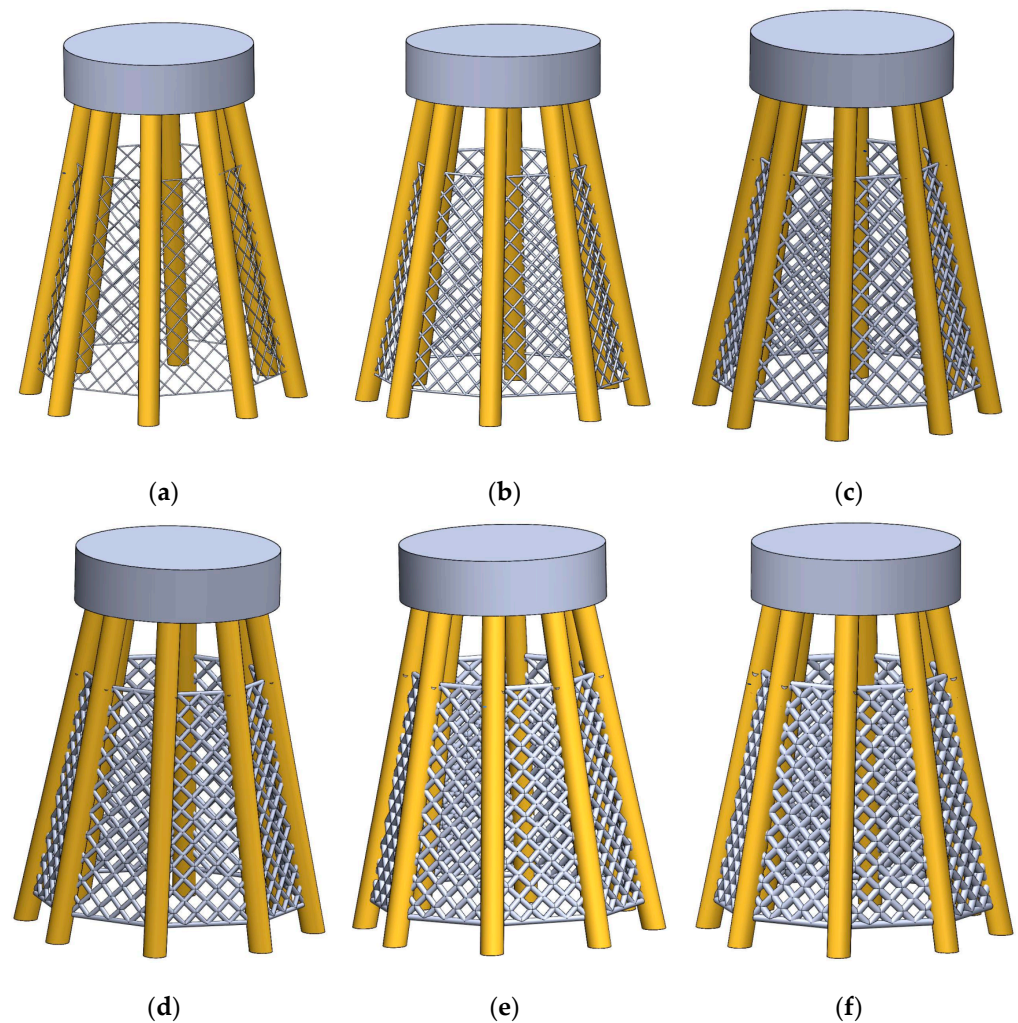


Figure 4. WT-NC model with different net solidities. (a) The net solidity is 0.1; (b) The net solidity is 0.2; (c) The net solidity is 0.3; (d) The net solidity is 0.4; (e) The net solidity is 0.5; (f) The net solidity is 0.6.

Based on the WT-NC models, a fluid domain is established to simulate their hydrodynamic characteristics. For the purpose of accurately representing the real water depth and minimizing the influence of boundary conditions, the dimensions of the fluid domain are set to $50 \times 150 \times 17$ m, as illustrated in Figure 5. In terms of boundary conditions, the y - z plane on the left side of the fluid domain is designated as the flow inlet, while the y - z plane on the right side serves as the flow outlet. A no-slip wall condition is applied to both the foundation and the side walls of the domain. The top surface of the domain is open. The flow velocity is set at a constant value of 2 m/s. Using this numerical model, the hydrodynamic loads of the WT-NC under currents and the surrounding flow field of the WT-NC are calculated and analyzed.

This article mainly analyzes the impact of additional netting on the offshore wind turbine foundation. Considering the actual use of netting in engineering, the range of net solidity selected in this article is 0.1–0.6, with a gradient of 0.1. In addition, to facilitate the hydrodynamic analysis of the foundation before and after the addition of netting, three models were established: a stand-alone offshore wind turbine foundation, a stand-alone net cage, and a foundation with a net cage. Considering different net solidities, a total of 13 load cases are included, as shown in Table 4.

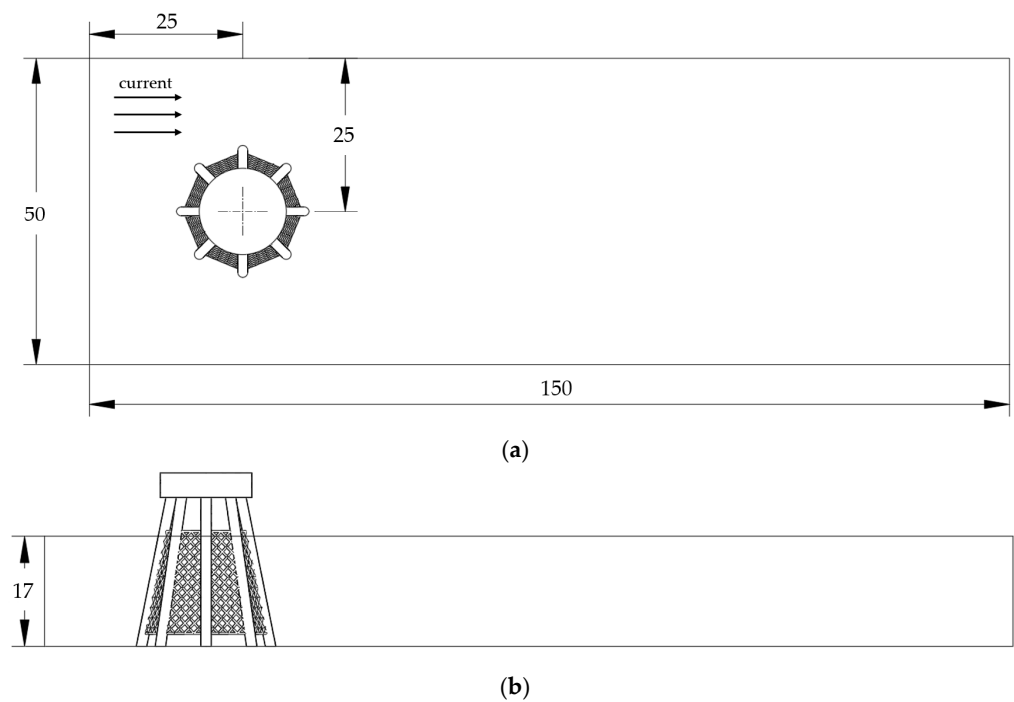


Figure 5. The computational domain. (a) The top view; (b) The side view.

Table 4. Load cases.

Cases	Net Solidities	Layout of Structure
1	/	stand-alone foundation
2	0.1	stand-alone cage
3	0.2	stand-alone cage
4	0.3	stand-alone cage
5	0.4	stand-alone cage
6	0.5	stand-alone cage
7	0.6	stand-alone cage
8	0.1	foundation with cage
9	0.2	foundation with cage
10	0.3	foundation with cage
11	0.4	foundation with cage
12	0.5	foundation with cage
13	0.6	foundation with cage

4.3. Grid Convergence Analysis

After dividing the grid, the numerical model was applied as shown in Figure 6. In order to evaluate the accuracy of the numerical model, a grid convergence analysis was conducted for the load case with a net solidity of 0.4. Four different grids were used to calculate the hydrodynamic loads of the piles and the netting, and the results are summarized in Table 5. From the table, it is evident that the hydrodynamic loads on the piles reached convergence in case 1, which indicates that the grid configuration of case 1 satisfies the numerical simulation requirements of fluid and piles. Moreover, employing a smaller mesh, the shape of the netting can be more accurately modeled, and the load on the netting reached convergence in case 3. Therefore, the grid of case 3 was used for subsequent simulations, and the selected grid was also adjusted proportionally for different net solidity models.

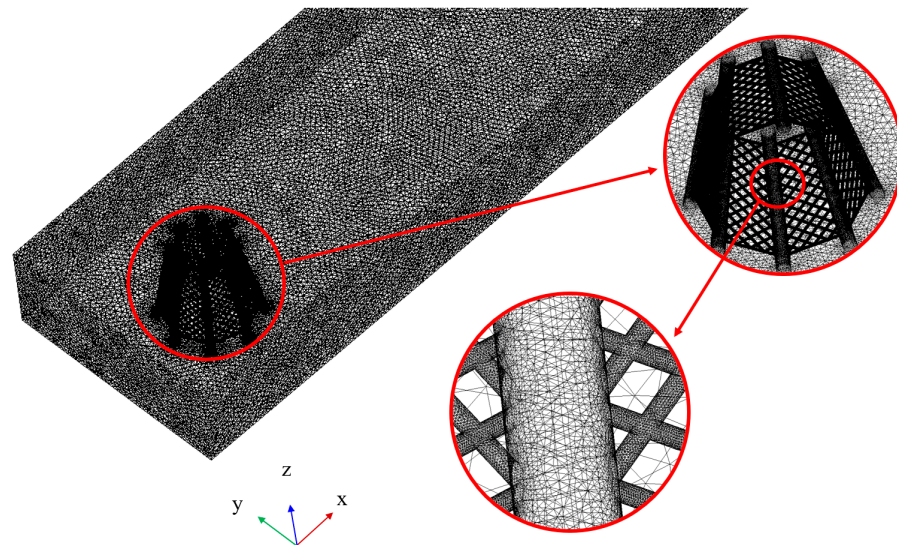


Figure 6. Computational domain and grids around the foundation.

Table 5. Grid convergence verification.

Case	Max. Size of Grid (m)	Min. Size of Grid (m)	Number of Grids	Load on Nets (kN)	Load on Piles (kN)
1	4	0.08	6,057,991	533.43	423.59
2	2	0.06	10,467,968	480.53	418.13
3	1	0.04	15,754,558	432.99	416.56
4	1	0.02	15,865,741	439.45	418.97

4.4. Numerical Model Verification

To validate the effectiveness of the numerical model, a numerical model with the same scale as the experimental physical model in [19] was established, as shown in Figure 7. The netting mesh used in the numerical model was a 4×4 grouping mesh, and the hydrodynamic loads on the middle pile and net panels in the numerical simulation and experiment were compared. It can be seen that the numerical simulation results are in good agreement with the experimental results, with a maximum error of 4.24%. This verifies the effectiveness of the numerical model proposed in this paper.

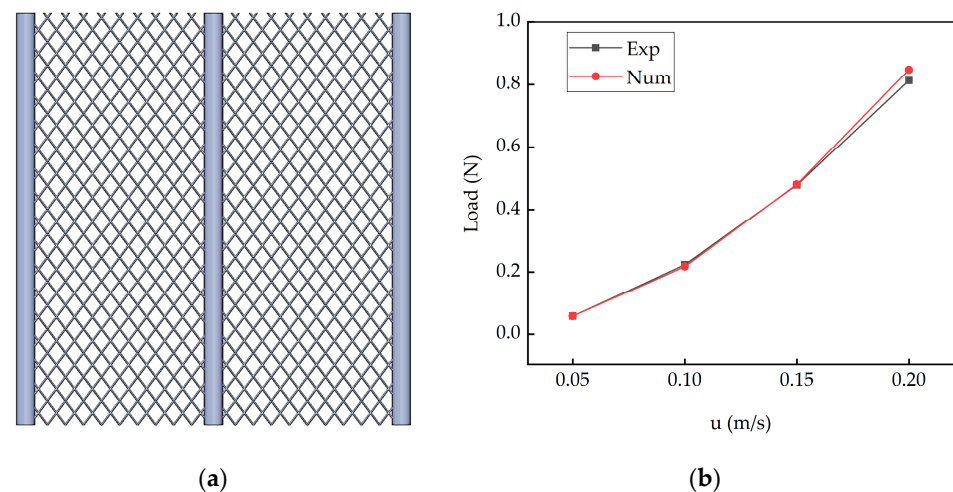


Figure 7. Numerical model verification. (a) Numerical model with the same scale as the physical model in [19]. (b) Comparison of experimental and numerical results of loads on the pile and net panels.

5. Results and Discussion

For the hydrodynamic characteristic analysis of the WT-NC, there are two aspects to consider. The first is the analysis of the surrounding flow field of the WT-NC, and the second is the analysis of the hydrodynamic loads on the WT-NC. By comparing the changes in the hydrodynamic loads of the offshore wind turbine foundation with and without the addition of netting, we can study the impacts of additional netting on the hydrodynamic loads of the foundation.

5.1. Flow Field around the Structure

In this study, a load case with a net solidity of 0.4 was selected to analyze the impact of additional netting on the flow field around the WT-NC. Figure 8 shows the flow field around the foundation with and without the addition of the netting. It is evident that the addition of the netting significantly alters the flow field around the foundation. Before the addition of the netting, the water was able to flow around the piles with limited resistance, and the interference between the piles was not pronounced. However, the net panels connect the eight piles into a single entity, reducing the flow space around the piles and dramatically improving the flow resistance of the foundation. As a result, the flow will pass through the sides of the foundation, causing an increase in flow velocity along the sides of the foundation. Inside and behind the foundation, most areas experience varying degrees of flow velocity decrease, particularly behind of the foundation where the flow speed decreases significantly due to the obstruction provided by the two layers of netting located upstream and downstream of the foundation. The addition of the netting greatly changes the distribution of the flow field around the foundation, which correspondingly alters the hydrodynamic loads on the foundation.

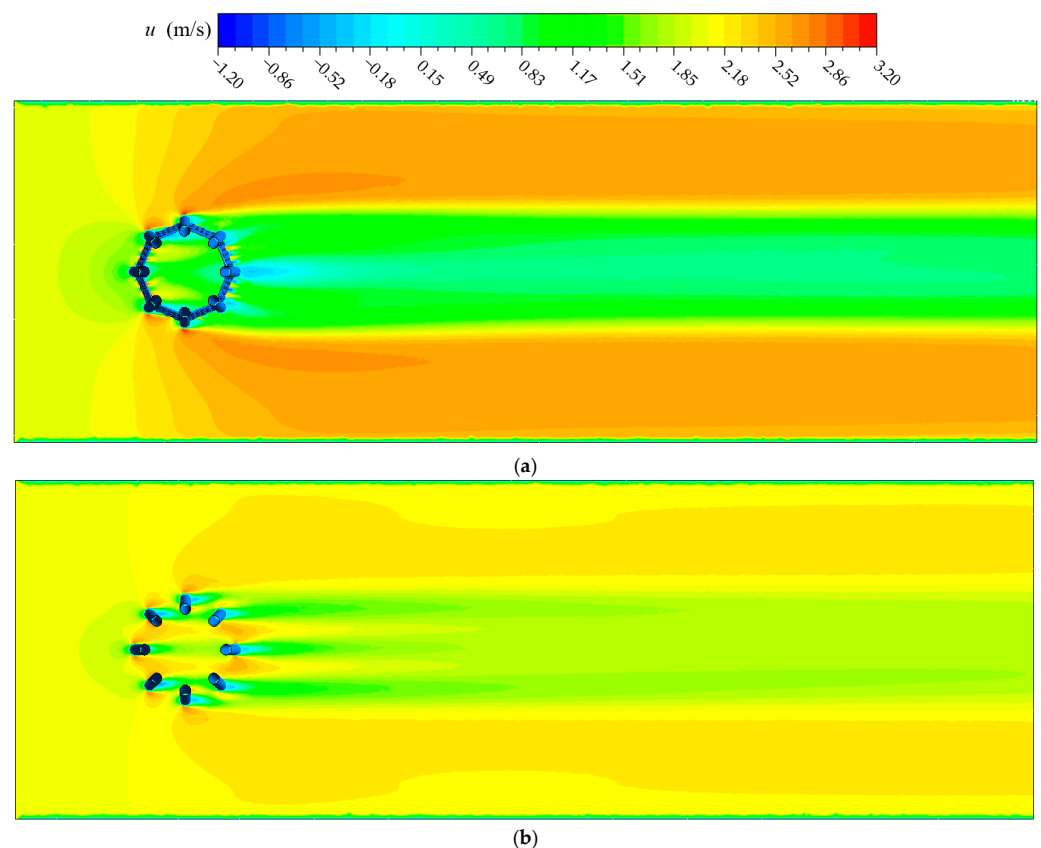


Figure 8. Flow velocity distribution around the foundation. (a) Foundation with cage; (b) stand-alone foundation.

A quantitative analysis of the surrounding flow field velocity of the WT-NC was conducted, wherein five lines were selected to extract the flow velocity components along the x-direction at the corresponding positions, as depicted in Figure 9. The resulting flow velocity curves along these five lines are plotted in Figure 10. Upon examination of the figure, notable changes in the overall flow velocity can be observed after traversing the WT-NC. Behind the foundation, the disturbed flow field stabilizes gradually after $x = 20$ m. The foundation exhibits left-right symmetry along the centerline, and the attenuation of flow velocity becomes more pronounced closer to the centerline of the foundation. At line 1 (corresponding to the centerline of the foundation), the flow velocity around the WT-NC eventually stabilizes at 0.62 m/s, with an attenuation of 69% compared to the inflow velocity. From line 1 to line 4, the stabilized flow velocity gradually increases, reaching approximately 1.25 m/s at line 4. Line 5 is located outside the foundation, and due to the flow diffraction effect, the flow velocity increases on both sides of the WT-NC. The flow velocity at line 5 eventually stabilizes at around 2.54 m/s.

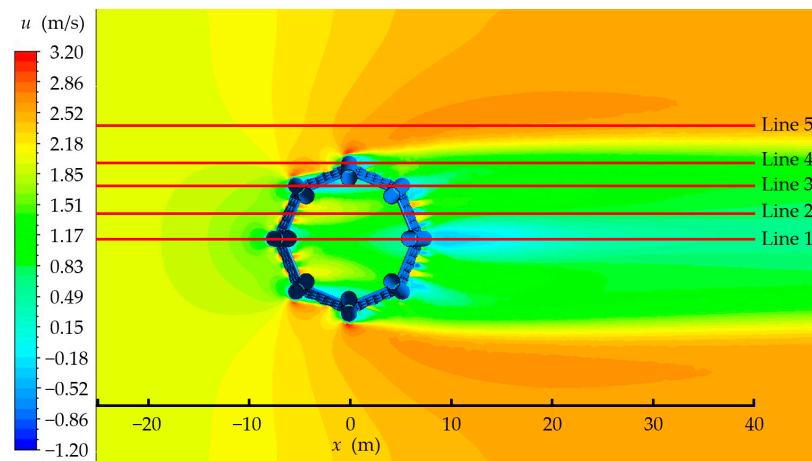


Figure 9. Positions of the lines around the foundation.

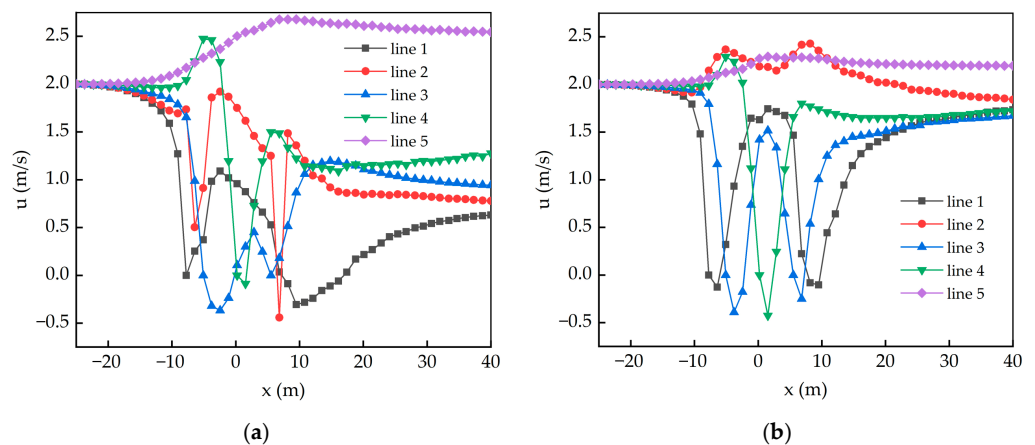


Figure 10. Flow velocity on the positions of the lines around the foundation. (a) Foundation with cage; (b) stand-alone foundation.

For the internal flow field of the WT-NC, the flow velocity attenuation is smaller compared to the flow field behind the WT-NC due to being only obstructed by the upstream section of the WT-NC. Specifically, lines 1, 2, and 3 pass through the interior of the foundation. The flow velocity attenuation is most pronounced at line 3, followed by line 1, and line 2 exhibits the smallest effect. This variation can be attributed to the specific obstructions encountered by each line. Line 1 is mainly obstructed by the mid-section pile of the upstream section of the foundation, while line 2 is primarily obstructed by the

net panel, which has a certain permeability and provides less obstruction. Additionally, line 2 also experiences an increase in flow velocity due to the flow diffraction effect at the sides of the piles. Therefore, the flow velocity attenuation effect at line 2 is relatively small. On the other hand, at line 3, the angle between the net panel and the x-axis is very small, resulting in an obstruction increase of the net panel. Line 3 is affected by the combined obstruction of the piles and the net panels, and since it is closer to the outer perimeter of the foundation, the flow can diffract around the exterior of the foundation. Hence, the flow velocity attenuation effect is most pronounced at line 3.

5.2. Overall Hydrodynamic Load Analysis of the Structure

Firstly, the changes in the overall hydrodynamic loads on the foundation after adding the netting were analyzed. The addition of the netting would increase the hydrodynamic loads on the foundation. Moreover, due to the mutual interference between the netting and the piles, the overall hydrodynamic loads on the WT-NC would be greater than the sum of the hydrodynamic loads on individual piles and netting. This amplification effect needs to be quantitatively evaluated. Therefore, the hydrodynamic loads were extracted for the individual foundation model and net cage model, and the hydrodynamic loads on the piles and netting were also extracted separately for the WT-NC model. By comparing them, the growth rate of the overall hydrodynamic load on the foundation are obtained, as well as the growth rate of the piles and netting after adding the netting.

The overall growth rate of the hydrodynamic load on the foundation after adding the netting with different net solidities is shown in Figure 11a. From this figure, it can be observed that the overall hydrodynamic load on the foundation significantly increases after adding the netting. As the net solidity increases, the overall hydrodynamic load of the foundation continues increasing. When the net solidity is 0.1, the growth rate of the hydrodynamic load is 49.61%. As the net solidity reaches 0.6, the growth rate reaches 204.75%, indicating that the hydrodynamic load on the WT-NC increases three-fold compared to the foundation without netting, which is worthy of attention.

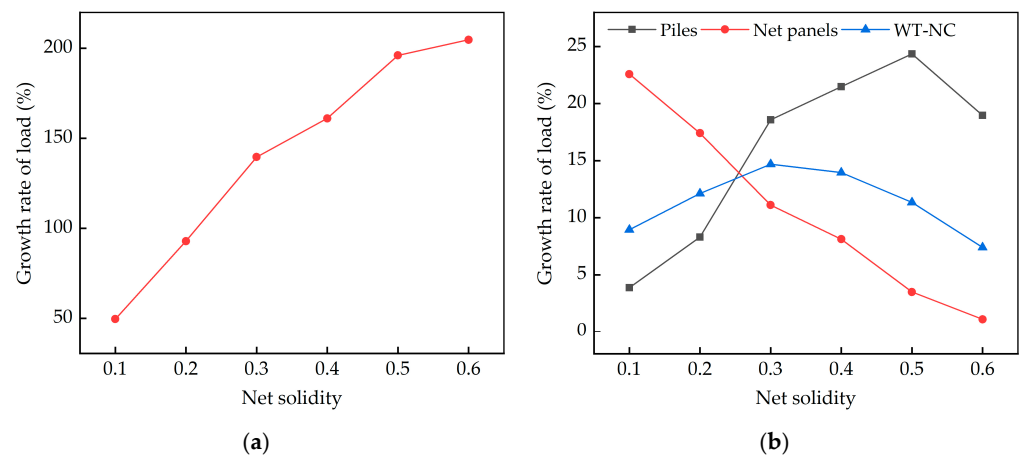


Figure 11. Growth rates of hydrodynamic loads on the foundation with different net solidities. (a) Growth rates of overall hydrodynamic load on the WT-NC compared with the stand-alone foundation; (b) growth rates of partial and overall hydrodynamic loads on the WT-NC.

To analyze the increase in hydrodynamic loads caused by the mutual interference between the netting and the piles, a detailed analysis is conducted on the growth rates of the hydrodynamic load on piles only, netting only, and the combination of both. The results are shown in Figure 11b. From this figure, it can be seen that all the hydrodynamic load growth rates are greater than zero, indicating that there is indeed a mutual interference effect between the piles and the netting, which leads to an increase in the hydrodynamic loads on the piles and the netting. Furthermore, after adding the netting, the hydrodynamic load growth rate of the piles initially increases with the increasing net solidities, reaching

a peak of 24.35% at the net solidity of 0.5, and then starts to decrease at the net solidity of 0.6. From the perspective of flow field analysis, the increase in net solidity reduces the flow space through the netting, which results in an increase in the flow velocity of the piles' upstream surface and an increase in its hydrodynamic load. However, when the net solidity is too high, the increasing attenuation effect of the front section of the foundation on the flow velocity will significantly reduce the hydrodynamic load on the rear piles. Therefore, the total hydrodynamic load on the piles decreases in the later stage.

As for the hydrodynamic load of the netting, the results show that the growth rate of the hydrodynamic load on the netting gradually decreases as the net solidity increases. The maximum growth rate is 22.58% when the solidity is the lowest. From the perspective of flow field analysis, as the net solidity increases, the influence of the piles on the upstream surface flow of the netting gradually decreases, since the piles were not changed, which leads to a gradual decrease in the hydrodynamic load growth rate of the netting.

Further adding the hydrodynamic loads of the netting and the piles together, we obtain the overall hydrodynamic loads of the WT-NC. It can be seen that the overall hydrodynamic load growth rate of the WT-NC increases first and then decreases as the net solidity increases. The peak value is 14.69% at the solidity of 0.3. This is also due to the interference of the netting on the flow field. The higher the net solidity, the greater the attenuation effect on the incoming flow velocity, which reduces the hydrodynamic loads on the downstream structure. Increasing the net solidity will not continuously increase the growth rate of the overall hydrodynamic load on the WT-NC.

In addition, considering that the hydrodynamic load coupling analysis of the offshore wind turbine foundation and aquaculture net cage is not yet mature in the industry, and the overall hydrodynamic load amplification factor of the WT-NC has a maximum value, in engineering calculations, the hydrodynamic load of the individual foundation and individual net cage can be directly superimposed; then, a safety factor can be considered to preliminarily evaluate the hydrodynamic load of the WT-NC.

5.3. Local Hydrodynamic Load Analysis of the Structure

From the overall structure hydrodynamic analysis, it can be clearly seen that the upstream section of the WT-NC has a shielding effect on the downstream structure. This will affect the distribution of hydrodynamic loads at various local positions of the WT-NC. It is necessary to conduct a specific analysis of the loads of the piles and net panels of the foundation. For ease of expression, the piles and net panels are numbered as shown in Figure 12. Considering the structural symmetry, it is only necessary to analyze five piles (piles I–V) and four net panels (net panels 1–4).

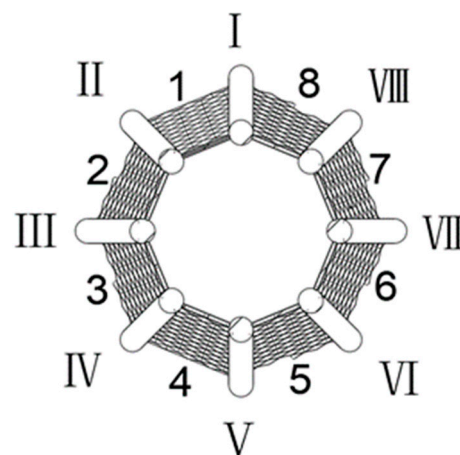


Figure 12. Numbers of piles and net panels of the WT-NC (I–VIII represent pile numbers, while 1–8 represent net panel numbers).

5.3.1. Hydrodynamic Loads on Piles

The curves of the hydrodynamic loads on piles I, II, III, IV, and V as a function of the net solidity are shown in Figure 13. From the figure, it can be seen that pile I, which is located in the middle of the upstream structure, bears the maximum hydrodynamic load, which increases continuously with the increase of the net solidity. At the solidity of 0.6, the load increases to 2.64 times its original size. The hydrodynamic loads on the other piles fluctuate slightly as the net solidity increases, with most loads within the range of $\pm 20\%$. The hydrodynamic loads on the other piles are not sensitive to changes in the net solidity.

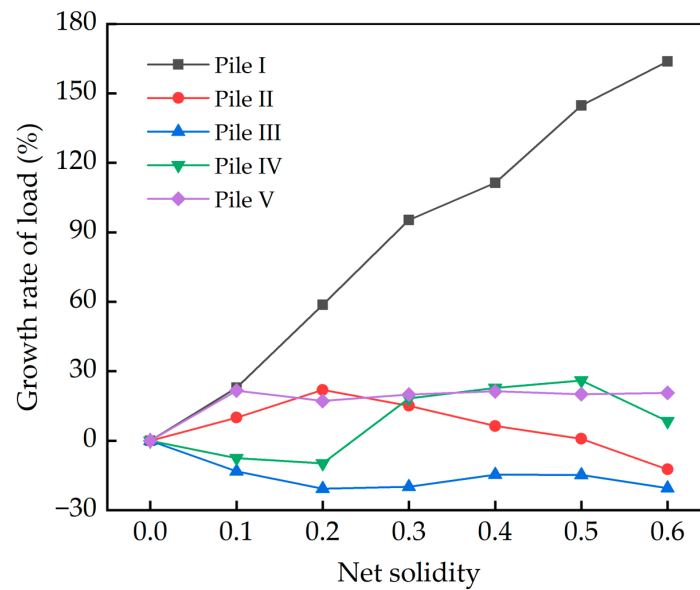


Figure 13. Growth rates of hydrodynamic loads on piles after the addition of netting with different net solidities.

From the analysis of the flow field, increasing the net solidity will improve the water-blocking effect of the structure and increase the hydrodynamic loads on the piles. Pile I is located in the middle of the upstream section of the WT-NC and is surrounded by the net panels, making it difficult for fluid to flow around. Therefore, the hydrodynamic load on pile I increases continuously with the increase of net solidity. However, the hydrodynamic loads on the piles on both sides is not significantly increased due to the space available for fluid to flow around the outer side. In fact, the hydrodynamic loads on these piles may decrease slightly due to the shielding effect of the upstream structure. As for the piles downstream of the foundation, the hydrodynamic load will increase due to the increase of net solidity, but it will also decrease due to the attenuation of the flow velocity caused by the upstream structure. Under these two effects, the change of the hydrodynamic loads on the downstream piles with the increase of net solidity is not significant. In engineering design, special attention should be paid to the hydrodynamic load on pile I, which is located in the middle of the upstream structure.

5.3.2. Hydrodynamic Loads on Net Panels

To perform a detailed analysis of the hydrodynamic loads on net panels 1, 2, 3, and 4, three hydrodynamic load curves for each net panel were drawn. The first curve represents the hydrodynamic loads on the net panels of the WT-NC, the second curve represents the hydrodynamic loads on the net panels of the stand-alone net cage, and the third curve represents the theoretical hydrodynamic loads of the net panels (based on the hydrodynamic load of the net panel when the net solidity is 0.1 and the Morison formula, assuming the hydrodynamic coefficients are constant, we can obtain the hydrodynamic loads of the net panels with different net solidities). The variation of the hydrodynamic

load of each net panel with different net solidities is shown in Figure 14. From the figure, it can be seen that the hydrodynamic load of each net panel mostly increases with the increase of net solidity, but the magnitude of the amplification varies among the different net panels.

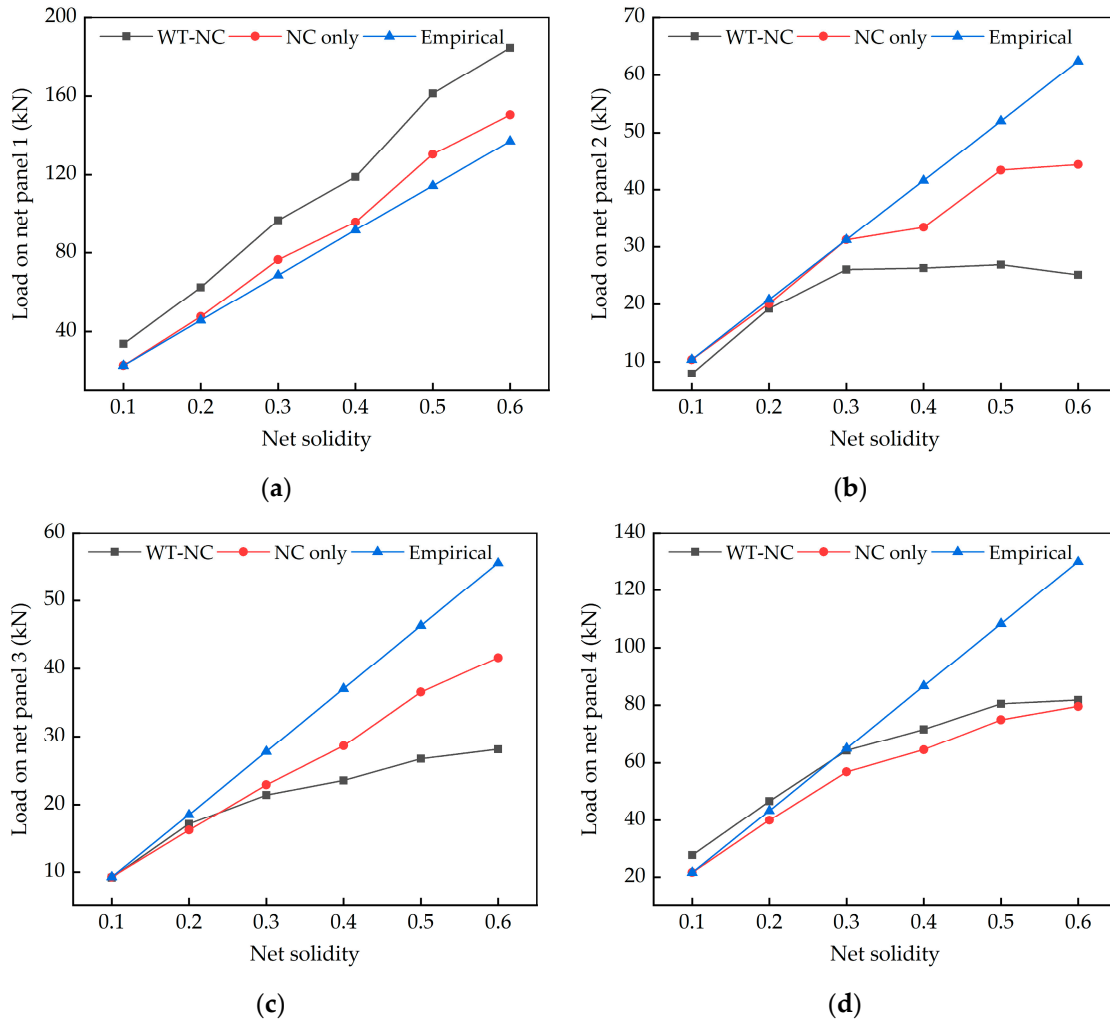


Figure 14. Hydrodynamic loads on net panels. (a) Load on net panel 1; (b) Load on net panel 2; (c) Load on net panel 3; (d) Load on net panel 4.

Based on the theoretical hydrodynamic load of the net panels, the growth rates of hydrodynamic loads on the net panels of the WT-NC and that of the stand-alone net cage can be obtained as shown in Figure 15. It can be seen that only the hydrodynamic load of the net panel 1 is increased compared to the theoretical curve, while the hydrodynamic loads of the other net panels are reduced. This is similar to the changes in the hydrodynamic loads of the piles. The net panel 1 is located in the middle of the upstream structure, with a small flow space around it; an increase in the solidity of the net panel will enhance the mutual interference effect between the netting wires, thereby increasing the hydrodynamic coefficient of the net panel. As a result, the hydrodynamic load of the net panel 1 is greater than the theoretical hydrodynamic load. On the other hand, for the other net panels, due to the shielding effect of the upstream structure, the flow velocity of the incoming flow will be reduced, which will reduce the hydrodynamic loads on the net panels, resulting in a lower hydrodynamic load than the theoretical curve. In other words, the increase in the hydrodynamic load coefficient caused by the increase in the net solidity is not as significant as the decrease in the hydrodynamic load caused by the reduction of the flow velocity, which plays a greater role in the changes in the hydrodynamic loads on the net panels. This

point can also be verified using the Morison formula, because the hydrodynamic load of the netting is proportional to the first order of the hydrodynamic load coefficient, but is also proportional to the square of the flow velocity. The presence of piles will reduce the flow space around the net panels, which will increase the resistance to flow, leading to a more significant reduction in the hydrodynamic loads on the net panels.

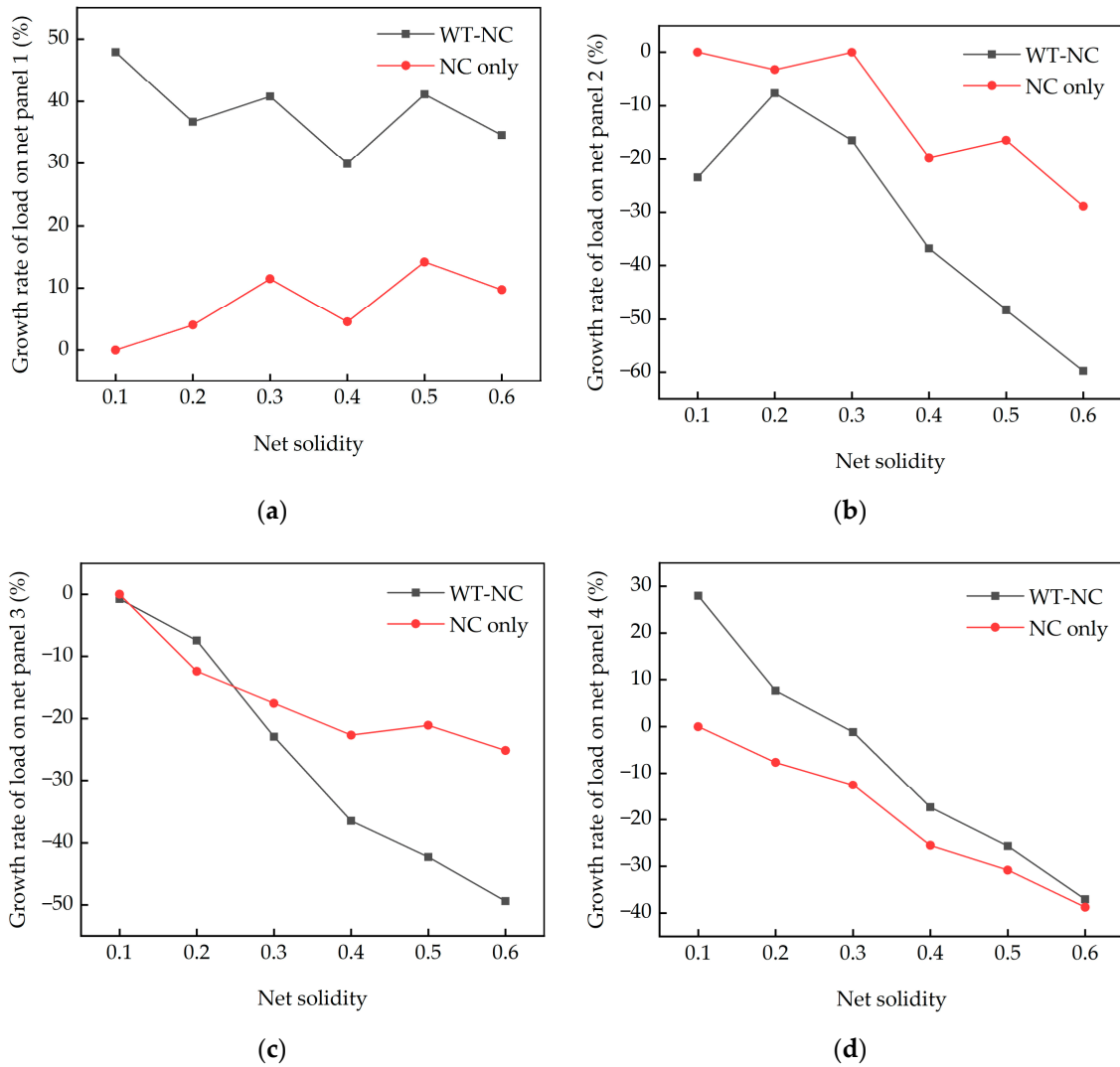


Figure 15. Growth rates of hydrodynamic loads on the net panels. (a) Growth rate of load no net panel 1; (b) Growth rate of load no net panel 2; (c) Growth rate of load no net panel 3; (d) Growth rate of load no net panel 4.

We quantitatively compared the growth rates of the hydrodynamic loads of the net panels. As shown in Figure 15, for net panel 1, the hydrodynamic load on the net panel of the WT-NC is significantly higher than that of the stand-alone net cage. The hydrodynamic load on net panel 1 of the WT-NC is increased within a range maintained at around 40% and a maximum value of 47.9%. The hydrodynamic load of the stand-alone net cage also shows some improvement, with an increase of about 10% and a maximum value of 14.15%. In addition, the growth rate of the hydrodynamic load on net panel 1 is relatively stable and insensitive to changes in net solidity. For net panels 2, 3 and 4, the hydrodynamic loads are attenuated to varying degrees compared to the theoretical curve, and the degree of attenuation increases with the increase in net solidity. The actual hydrodynamic load on the net panels reaches a minimum when attenuated to 40.25% of the theoretical hydrodynamic load, which occurs at net panel 2. Among them, the hydrodynamic load attenuation of

net panel 2 and net panel 3 of the WT-NC is greater than that of the stand-alone net cage, indicating that the presence of piles makes the attenuation effect of the flow velocity more significant for net panel 2 and net panel 3. However, this phenomenon is reversed for net panel 4, where the results show that the hydrodynamic load increase of net panel 4 in the WT-NC is more obvious. This situation is similar to that of net panel 1, where the presence of piles reduces the surrounding flow space around the net panel, resulting in a greater hydrodynamic load.

However, the hydrodynamic loads on the net panels still need to be borne by the piles. By combining the hydrodynamic loads on each pile and net panel of the WT-NC, it can be seen that after the addition of the netting, the hydrodynamic load borne by pile I faces a huge increase, as the hydrodynamic loads are concentrated on the upstream structure. According to the results, the direct hydrodynamic load borne by pile I will increase to 2.64 times that without the netting. In addition, the piles also need to indirectly bear the hydrodynamic loads transmitted by the net panels. Taking two pieces of net panels of the upstream structure as an example, the hydrodynamic loads are borne by three piles of the upstream structure, while the middle pile, i.e., pile I, bears a greater load. Assuming it is 50% for preliminary estimation, the hydrodynamic load of pile I will further increase 6.32 times, which will significantly increase the risk of structural failure and is especially worthy of attention. During engineering design, it is necessary to analyze the hydrodynamic loads of each pile in detail, focusing on the upstream section of the structure to ensure structural safety.

5.4. Feasibility Analysis

5.4.1. Economic Analysis

To explore the feasibility of the proposed scheme in this study, a preliminary economic analysis was conducted on the project.

The offshore wind farm project discussed in this paper is located in Zhoushan City, Zhejiang Province, China. Considering the indigenous fish species in the Zhejiang region, strong resistance to currents, wide tolerance to salinity and temperature, mature aquaculture techniques, and high economic value, the project selected Blackhead Seabream (*Acanthopagrus schlegelii*) as the target species for cultivation. Additionally, Blackhead Seabream feed on shellfish and algae, effectively inhibiting the attachment of marine organisms to the netting, thereby avoiding increased hydrodynamic load on the netting due to biofouling. Based on the net mesh size, the average weight of fish fry in this project is 150 g. The effective culture water volume in the cage of this project is approximately 2400 m³. Considering the survival rate of fish fry, the stocking density of fish per cubic meter of culture water is 30, with a culture period of 1 year and an expected harvest size of 500 g.

The aquaculture cage production costs of this project mainly include three aspects: breeding equipment and cage structure costs, installation costs, and aquaculture costs, as shown in Table 6. It is worth mentioning that there are differences in net panel connection structures between operational wind turbines and non-operational ones, resulting in different costs. For non-operational wind turbines, the net panel connection components can be welded to the piles during the manufacturing process. However, for operational wind turbines, underwater welding operations are challenging, and the welding quality is difficult to guarantee. Therefore, the net panels are fixed to the piles using clamps and other connectors. These differences result in different structural and installation costs. Therefore, the table also presents two options for discussion, with the content in parentheses representing Option 2, applicable to operational wind turbines. The breeding equipment and structures include feeding machines, feed storage bins, maintenance suspension bridges, netting, netting connectors, and other accessories. The cage installation costs include netting installation, netting connector installation, and maintenance suspension bridge installation. The specific costs of installation primarily include vessel costs and diver-related personnel costs.

Table 6. Initial capital investment for aquaculture cages.

Item	Component	Quantity	Price (10 ³ CNY)
Breeding equipment and structure costs	Feeding machine	2 units	60
	Feed storage bin	2 units	50
	Maintenance suspension bridge	1 unit	150
	Netting	650 kg	234
	Eye plate	72 units	7.2
	Connecting steel	64 units	12.8
	Clamping hoop (Option 2)	72 units	288
	Other accessories	1 unit	10
	Subtotal		524 (812) *
Installation cost	Netting installation	1 unit	268
	Suspension bridge installation	1 unit	100
	Connection piece installation (Option 2)	1 unit	360
	Subtotal		368 (728) *
Total costs			892 (1540) *

* The content in parentheses represents Option 2, applicable to operational wind turbines.

Aquaculture costs mainly include fish fry costs, fish caretaker costs, feed costs, netting cleaning costs, and fish capture costs. Due to the availability of vessel resources in the offshore wind farm itself, including the regular transportation of feed using maintenance vessels from the offshore wind farm, and the ability to utilize the wind turbine foundation platform to arrange feeding machines and feed storage bins for automated feeding, vessel costs can be avoided. The project is equipped with an automatic feeding device, and the wind turbine platform has a small crane for feed transportation, which can be performed by two caretakers. The unit price of fish fry in this project is CNY 8, the feed conversion ratio is 1.2, and the costs for netting cleaning and fish capture are based on annual leasing.

On the other hand, for the offshore wind turbine, as mentioned above, the additional netting will increase the hydrodynamic load on the foundation, posing challenges to structural safety and possibly requiring reinforcement of the foundation. However, the need for structural reinforcement requires further analysis of the overall wind turbine structure. The strength design of the wind turbine foundation needs to verify the bending stress generated by the wind and wave loads in the structure, primarily considering two different load cases: the ultimate load under extreme conditions and the fatigue load under operational conditions. In these two load cases, the hydrodynamic load plays a different role. Under operational conditions, the wind turbine generates significant loads, while the hydrodynamic load is relatively small, making the wind load the primary factor. Under extreme conditions, the hydrodynamic load plays a more significant role in the overall load of the wind turbine. During these conditions, the wind turbine is in a shutdown state, with reduced wind loads and increased hydrodynamic loads. However, due to the large moment arm of the upper wind loads compared to the foundation hydrodynamic load, especially in shallow water depths, the bending moment generated by the wind loads will still be much greater than that of the hydrodynamic load, thus remaining the main factor. Additionally, typically, the strength design of the wind turbine foundation is dependent on the fatigue load under operational conditions, allowing for a larger design margin for extreme conditions. Moreover, considering the shallow water depth and the high rigidity of the foundation structure in this project, although the netting may significantly increase the hydrodynamic load on the foundation, the actual enhancement of the structure may be limited. Based on this, the cost for reinforcing the wind turbine foundation is not considered in this study as a preliminary analysis.

Regarding the annual income from aquaculture, the fish species cultivated in this project have a high level of technical maturity, with a survival rate of up to 90%. The annual fish yield is 38,900 kg, with a price of CNY 90 per kilogram. The annual production value and profit of the aquaculture are shown in Table 7. For non-operational and operational

offshore wind turbines, the return on investment for integrating an aquaculture cage can reach 191.14% and 110.71%, respectively, indicating excellent economic viability of the integrated aquaculture cage industry. Additionally, the water depth of this project is only about 10 m, with a culture water volume of 2400 m³. The annual aquaculture profit can reach CNY 1.705 million. In comparison, for jacket foundations with water depths of over 50 m, the effective culture water volume can reach tens of thousands of cubic meters, and the annual aquaculture profit can amount to tens of millions. This is similar to the annual profit generated by 10 MW wind turbine power generation in China, showcasing tremendous prospects for the development of integrated aquaculture cages in deep-sea environments. While increasing water depth also increases the hydrodynamic load on the foundation, thereby increasing structural costs, it cannot be denied that the offshore wind power integrated aquaculture cage industry has enormous development potential.

Table 7. Annual aquaculture cost and revenue.

Item	Component	Quantity	Price (10 ³ CNY)
Annual aquaculture cost	Fish fry	72,000 units	576
	Staff	1 unit	96
	Fish feed	38,900 kg	389
	Netting cleaning	1 unit	50
	Fish capture	1 unit	100
	Subtotal		1211
Annual revenue	Fish yield weight	32,400 kg	2916
Return on investment	Annual profit		1705
	Return on investment		191.14% (110.71%) *

* The content in parentheses represents Option 2, applicable to operational wind turbines.

5.4.2. Advantages of the Integrated Development of Offshore Wind Power and Marine Aquaculture

The integrated development model of offshore wind power and marine aquaculture presents several advantages. For the offshore wind power industry, integration brings additional economic benefits and reduces the cost of electricity generation. For the marine aquaculture industry, the structural support provided by wind turbine foundations significantly enhances the resistance of cages against wind and waves, improving structural safety. The wind turbine platform can serve as a management platform for aquaculture, and the offshore wind farm provides power and information transmission capabilities, addressing the energy needs of marine aquaculture and enabling remote monitoring of aquaculture cage operations. Additionally, the use of wind farm service vessels can greatly enhance the operational capacity of marine aquaculture. Compared to traditional floating net cages, integrated net cages offer improved safety and higher levels of automation, resulting in lower costs. Furthermore, compared to large-scale deep-sea aquaculture cages, integrated cages can significantly reduce costs while benefiting from power and information transmission capabilities.

In addition, the integration of offshore wind power and marine aquaculture in terms of aspects such as space, structure, and functionality resolves conflicts in the use of ocean space, increases the utilization of ocean resources, achieves mutually beneficial upgrades for both industries, and drives the healthy development of the two sectors. It represents a new industrial model and future direction for the efficient and sustainable use of maritime resources.

Against the backdrop of cost reduction and efficiency improvement in offshore wind power, the integration of offshore wind power with other marine industries is an effective way to lower overall costs. Compared to the integration of offshore wind power with other industries such as wave energy, tidal energy, offshore solar power, offshore oil and gas, desalination, hydrogen production from seawater, and energy storage, the integration with the marine aquaculture industry has higher technological and industrial maturity

at present, making it more feasible. On 25 July 2023, the world's first jacket offshore wind turbine-integrated aquaculture cage was successfully installed on the offshore wind farm in Yangjiang city, Guangdong province, China, further validating the feasibility of the integrated development model of offshore wind power and marine aquaculture and providing strong support for the scheme proposed in this paper.

6. Conclusions

This article focuses on proposing a design scheme for a multi-pile-support offshore wind turbine foundation integrated with an aquaculture net cage, based on an offshore wind farm project. Firstly, the impact of the additional net cage on the offshore wind turbine was preliminarily analyzed based on structural dynamics and offshore wind turbine design theory. Subsequently, using the CFD method, the hydrodynamic loads and surrounding flow field of the offshore wind turbine foundation with the net cage under flow were analyzed. Finally, a preliminary feasibility analysis of the scheme was conducted. The following conclusions were drawn:

- (1) The integration of the net cage brings about additional hydrodynamic loads on the offshore wind turbine foundation, which poses significant challenges to the bearing capacity, strength, and displacement of the foundation. However, the impact on the structural frequency of the wind turbine can be considered negligible.
- (2) With the addition of the net cage, the netting connects the piles into a single entity, significantly enhancing the structure's resistance to the flow. The flow field around the foundation undergoes significant changes, including significant flow velocity attenuation inside and behind the foundation, while the flow velocity on both sides of the foundation increases.
- (3) With the addition of the net cage, the overall hydrodynamic load on the foundation increases significantly with an increase in net solidity. The maximum growth rate reaches 204.75% when the net solidity is 0.6. The mutual interference between the netting and the foundation increases the hydrodynamic load acting on both, resulting in a more substantial increase in the hydrodynamic load on the structure.
- (4) With the addition of the net cage, the hydrodynamic load on the foundation is concentrated at the upstream section of the structure. As the net solidity increases, the maximum increase in hydrodynamic load for a single pile reaches 6.32 times its original value, posing a significant danger.
- (5) For non-operational and operational offshore wind turbines, the return on investment for integrating an aquaculture cage can reach 191.14% and 110.71%, respectively. The integrated development model of offshore wind power and marine aquaculture presents many advantages, enormous development potential, and good feasibility, representing a new industrial model and future direction for the efficient and sustainable use of maritime resources.

7. Future Work

This paper provides a preliminary analysis of the impact of additional net cages on offshore wind turbines. However, the analysis process is based on certain assumptions, and there are still many limitations that require further research.

- (1) The fluid-structure interaction analysis of the flexible netting is a challenging task [20,38]. In this study, the deformation of the netting was neglected, which introduces some errors in the hydrodynamic load analysis of the netting. Moreover, it also restricts the calculation of the tension exerted by the netting on the piles, thus preventing a strength analysis of the piles.
- (2) This article only focuses on the current and conducts a quasi-static analysis of the structural hydrodynamic load, without considering the dynamic effects of wave loads. The dynamic effects of waves and the combined effects of waves and currents on the structure need to be further investigated.

- (3) Conducting a comprehensive analysis of offshore wind turbines using computational fluid dynamics (CFD) is a challenging task [56–58]. In this study, the offshore wind turbine foundation was separated from the wind turbine, and only the influence of the hydrodynamic load of the netting on the offshore wind turbine foundation was analyzed, without considering the coupling effects between the wind and hydrodynamic loads acting on the offshore wind turbine.

Author Contributions: Conceptualization, Z.T. and R.Z.; methodology, Z.T. and C.Z.; software, Z.T. and H.L.; validation, Z.T., C.Z. and H.L.; formal analysis, Z.T.; investigation, Z.T., C.Z. and H.L.; data curation, Z.T. and C.Z.; writing—original draft preparation, Z.T.; writing—review and editing, R.Z. and C.Z.; visualization, Z.T.; supervision, R.Z.; project administration, R.Z.; funding acquisition, R.Z. All authors have read and agreed to the published version of the manuscript.

Funding: This research was funded by the Key Area Research and Development Program of Guangdong Province (Grant No.: 2022B0707030001), the Hainan Provincial Joint Project of Sanya Yazhou Bay Science and Technology City (Grant No.: 2021JJLH0098), and the Special Fund Project for the Development of Guangdong Province’s Marine Economy (Six Major Marine Industries) (Grant No.: Yue Ziranzhihe [2022] 23).

Institutional Review Board Statement: Not applicable.

Informed Consent Statement: Not applicable.

Data Availability Statement: Not applicable.

Conflicts of Interest: The authors declare no conflict of interest.

References

1. GWEC. *Global Wind Report 2023*; GWEC: Brussels, Belgium, 2023.
2. Jahani, K.; Langlois, R.G.; Afagh, F.F. Structural dynamics of offshore Wind Turbines: A review. *Ocean Eng.* **2022**, *251*, 111136. [[CrossRef](#)]
3. Wang, L.; Kolios, A.; Liu, X.; Venetsanos, D.; Cai, R. Reliability of offshore wind turbine support structures: A state-of-the-art review. *Renew. Sustain. Energy Rev.* **2022**, *161*, 112250. [[CrossRef](#)]
4. Jalbi, S.; Bhattacharya, S. Concept design of jacket foundations for offshore wind turbines in 10 steps. *Soil. Dyn. Earthq. Eng.* **2020**, *139*, 106357. [[CrossRef](#)]
5. Abbas Ebrahimi, M.S. Transient response of the flexible blade of horizontal-axis wind turbines in wind gusts and rapid yaw changes. *Energy* **2017**, *145*, 261–275. [[CrossRef](#)]
6. Suja-Thauvin, L.; Krokstad, J.R.; Bachynski, E.E.; de Ridder, E.J. Experimental results of a multimode monopile offshore wind turbine support structure subjected to steep and breaking irregular waves. *Ocean Eng.* **2017**, *146*, 339–351. [[CrossRef](#)]
7. Faria Sharmin, M.H. Influence of soil-structure interaction on seismic responses of offshore wind turbine considering earthquake incident angle. *Earthq. Struct.* **2017**, *13*, 39–50. [[CrossRef](#)]
8. *DNVGL-ST-0437*; Loads and Site Conditions for Wind Turbines. DNVGL AS: Oslo, Norway, 2016.
9. *ABS. Guide of Building and Classing Floating Offshore Wind Turbines*; ABS: Spring, TX, USA, 2020.
10. O’Shea, R.; Collins, A.; Howe, C. Offshore Multi-use setting: Introducing integrative assessment modelling to alleviate uncertainty of developing Seaweed Aquaculture inside Wind Farms. *Environ. Chall.* **2022**, *8*, 100559. [[CrossRef](#)]
11. Naylor, R.L.; Goldburg, R.J.; Primavera, J.H.; Kautsky, N.; Beveridge, M.C.; Clay, J.; Folke, C.; Lubchenco, J.; Mooney, H.; Troell, M. Effect of aquaculture on world fish supplies. *Nature* **2000**, *405*, 1017–1024. [[CrossRef](#)]
12. Naylor, R.L.; Hardy, R.W.; Buschmann, A.H.; Bush, S.R.; Cao, L.; Klinger, D.H.; Little, D.C.; Lubchenco, J.; Shumway, S.E.; Troell, M. A 20-year retrospective review of global aquaculture. *Nature* **2021**, *591*, 551–563. [[CrossRef](#)]
13. *FAO. The State of World Fisheries and Aquaculture 2022. Towards Blue Transformation*; FAO: Rome, Italy, 2022.
14. Froehlich, H.E.; Gentry, R.R.; Halpern, B.S. Global change in marine aquaculture production potential under climate change. *Nat. Ecol. Evol.* **2018**, *2*, 1745–1750. [[CrossRef](#)]
15. Schubel, J.R.; Thompson, K. Farming the Sea: The only way to meet humanity’s future food needs. *Geohealth* **2019**, *3*, 238–244. [[CrossRef](#)]
16. Zhao, Y.; Guan, C.; Bi, C.; Liu, H.; Cui, Y. Experimental investigations on hydrodynamic responses of a semi-submersible offshore fish farm in waves. *J. Mar. Sci. Eng.* **2019**, *7*, 238. [[CrossRef](#)]
17. Zhao, Y.; Liu, H.; Bi, C.; Cui, Y.; Guan, C. Numerical study on the flow field inside and around a semi-submersible aquaculture platform. *Appl. Ocean Res.* **2021**, *115*, 102824. [[CrossRef](#)]
18. Jin, J.; Su, B.; Dou, R.; Luan, C.; Li, L.; Nygaard, I.; Fonseca, N.; Gao, Z. Numerical modelling of hydrodynamic responses of Ocean Farm 1 in waves and current and validation against model test measurements. *Mar. Struct.* **2021**, *78*, 103017. [[CrossRef](#)]

19. Yang, H.; Xu, Z.; Bi, C.; Zhao, Y.P. Numerical modeling of interaction between steady flow and pile-net structures using a one-way coupling model. *Ocean Eng.* **2022**, *254*, 111362. [[CrossRef](#)]
20. Fan, Z.; Liang, Y.; Zhao, Y. Review of the research on the hydrodynamics of fishing cage nets. *Ocean Eng.* **2023**, *276*, 114192. [[CrossRef](#)]
21. Xu, Z.; Qin, H. Fluid-structure interactions of cage based aquaculture: From structures to organisms. *Ocean Eng.* **2020**, *217*, 107961. [[CrossRef](#)]
22. Loland, G. Current Forces on and Flow through Fish Farms. Ph.D. Thesis, The Norwegian Institute of Technology, Trondheim, Norway, 1991.
23. Tsukrov, I.; Drach, A.; DeCew, J.; Swift, M.R.; Celikkol, B. Characterization of geometry and normal drag coefficients of copper nets. *Ocean Eng.* **2011**, *38*, 1979–1988. [[CrossRef](#)]
24. Tang, H.; Xu, L.; Hu, F. Hydrodynamic characteristics of knotted and knotless purse seine netting panels as determined in a flume tank. *PLoS ONE* **2018**, *13*, e192206. [[CrossRef](#)]
25. Lader, P.; Enerhaug, B.; Fredheim, A.; Klebert, P.; Pettersen, B. Forces on a cruciform/sphere structure in uniform current. *Ocean Eng.* **2014**, *82*, 180–190. [[CrossRef](#)]
26. Moe-Føre, H.; Lader, P.F.; Lien, E.; Hopperstad, O.S. Structural response of high solidity net cage models in uniform flow. *J. Fluids Struct.* **2016**, *65*, 180–195. [[CrossRef](#)]
27. Li, L.; Fu, S.; Xu, Y.; Wang, J.; Yang, J. Dynamic responses of floating fish cage in waves and current. *Ocean Eng.* **2013**, *72*, 297–303. [[CrossRef](#)]
28. Shainee, M.; DeCew, J.; Leira, B.J.; Ellingsen, H.; Fredheim, A. Numerical simulation of a self-submersible SPM cage system in regular waves with following currents. *Aquac. Eng.* **2013**, *54*, 29–37. [[CrossRef](#)]
29. Faltinsen, O.M.; Shen, Y. Wave and current effects on floating fish farms. *J. Mar. Sci. Appl.* **2018**, *17*, 284–296. [[CrossRef](#)]
30. Takagi, T.; Shimizu, T.; Suzuki, K.; Hiraishi, T.; Yamamoto, K. Validity and layout of “NaLA”: A net configuration and loading analysis system. *Fish. Res.* **2004**, *66*, 235–243. [[CrossRef](#)]
31. Cheng, H.; Li, L.; Ong, M.C. Comparative study of five commonly used gravity type fish cages under pure current conditions. *Ocean Eng.* **2022**, *250*, 110977. [[CrossRef](#)]
32. Zhao, Y.; Bi, C.; Dong, G.; Gui, F.; Cui, Y.; Guan, C.; Xu, T. Numerical simulation of the flow around fishing plane nets using the porous media model. *Ocean Eng.* **2013**, *62*, 25–37. [[CrossRef](#)]
33. Zhao, Y.; Bi, C.; Dong, G.; Gui, F.; Cui, Y.; Xu, T. Numerical simulation of the flow field inside and around gravity cages. *Aquac. Eng.* **2013**, *52*, 1–13. [[CrossRef](#)]
34. Bui, C.M.; Ho, T.X.; Khieu, L.H. Numerical study of a flow over and through offshore fish cages. *Ocean Eng.* **2020**, *201*, 107140. [[CrossRef](#)]
35. Martin, T.; Kamath, A.; Bihs, H. A Lagrangian approach for the coupled simulation of fixed net structures in a Eulerian fluid model. *J. Fluids Struct.* **2020**, *94*, 102962. [[CrossRef](#)]
36. Bi, C.; Zhao, Y.; Dong, G.; Zheng, Y.; Gui, F. A numerical analysis on the hydrodynamic characteristics of net cages using coupled fluid–structure interaction model. *Aquac. Eng.* **2014**, *59*, 1–12. [[CrossRef](#)]
37. Chen, H.; Christensen, E.D. Development of a numerical model for fluid-structure interaction analysis of flow through and around an aquaculture net cage. *Ocean Eng.* **2017**, *142*, 597–615. [[CrossRef](#)]
38. Cheng, H.; Ong, M.C.; Li, L.; Chen, H. Development of a coupling algorithm for fluid-structure interaction analysis of submerged aquaculture nets. *Ocean Eng.* **2022**, *243*, 110208. [[CrossRef](#)]
39. Yao, Y.; Chen, Y.; Zhou, H.; Yang, H. Numerical modeling of current loads on a net cage considering fluid–structure interaction. *J. Fluids Struct.* **2016**, *62*, 350–366. [[CrossRef](#)]
40. Lacroix, D.; Pioch, S. The multi-use in wind farm projects: More conflicts or a win-win opportunity? *Aquat. Living Resour.* **2011**, *24*, 129–135. [[CrossRef](#)]
41. Huang, C.; Afero, F.; Hung, C.; Chen, B.; Nan, F.; Chiang, W.; Tang, H.; Kang, C. Economic feasibility assessment of cage aquaculture in offshore wind power generation areas in Changhua County, Taiwan. *Aquaculture* **2022**, *548*, 737611. [[CrossRef](#)]
42. Benjamins, S.; Masden, E.; Collu, M. Integrating wind turbines and fish farms: An evaluation of potential risks to marine and coastal bird species. *J. Mar. Sci. Eng.* **2020**, *8*, 414. [[CrossRef](#)]
43. Tang, H.; Chiang, W.; Nan, F. Engineering feasibility assessment of cage aquaculture in offshore wind power generation areas in Taiwan. *Sustainability* **2022**, *14*, 11705. [[CrossRef](#)]
44. Li, N.; Shi, W.; Han, X.; Li, X.; Verma, A.S.; Liu, C. Dynamic analysis of an integrated offshore structure comprising a jacket-supported offshore wind turbine and aquaculture steel cage. *Ocean Eng.* **2023**, *274*, 114059. [[CrossRef](#)]
45. Zhai, Y.; Zhao, H.; Li, X.; Shi, W. Hydrodynamic responses of a barge-type floating offshore wind turbine integrated with an aquaculture cage. *J. Mar. Sci. Eng.* **2022**, *10*, 854. [[CrossRef](#)]
46. Zhang, C.; Wang, S.; Cui, M.; Liu, H.; Liu, A.; Xu, J.; Xie, S. Modeling and dynamic response analysis of a submersible floating offshore wind turbine integrated with an aquaculture cage. *Ocean Eng.* **2022**, *263*, 112338. [[CrossRef](#)]
47. Lei, Y.; Zhao, S.X.; Zheng, X.Y.; Li, W. Effects of fish nets on the nonlinear dynamic performance of a floating offshore wind turbine integrated with a steel fish farming cage. *Int. J. Struct. Stab. Dyn.* **2020**, *20*, 2050042. [[CrossRef](#)]
48. Miao, Y.; Ding, J.; Tian, C.; Chen, X.; Fan, Y. Experimental and numerical study of a semi-submersible offshore fish farm under waves. *Ocean Eng.* **2021**, *225*, 108794. [[CrossRef](#)]

49. Shih, T.H.; Liou, W.W.; Shabbir, A.; Yang, Z.; Zhu, J. A new k- ϵ eddy viscosity model for high Reynolds number turbulent flows. *Comput. Fluids* **1995**, *3*, 227238.
50. DNVGL. Support structures for wind turbines. In *DNVGL-ST-0126*; DNVGL AS: Oslo, Norway, 2018.
51. Huang, L.; Li, Y.; Wang, G.; Wang, Y.; Wu, Q.; Jia, M.; Wan, R. An improved Morison hydrodynamics model for knotless nets based on CFD and metamodelling methods. *Aquac. Eng.* **2022**, *96*, 102220. [[CrossRef](#)]
52. Wang, G.; Martin, T.; Huang, L.; Bihs, H. Numerical investigation of the hydrodynamics of a submersible steel-frame offshore fish farm in regular waves using CFD. *Ocean Eng.* **2022**, *256*, 111528. [[CrossRef](#)]
53. Li, L.; Ong, M.C. A preliminary study of a rigid semi-submersible fish farm for open seas. *Int. Conf. Offshore Mech. Arct. Eng.* **2017**, 57779, V009T12A044.
54. Moe, H.; Fredheim, A.; Hopperstad, O.S. Structural analysis of aquaculture net cages in current. *J. Fluids Struct.* **2010**, *26*, 503–516. [[CrossRef](#)]
55. Endresen, P.C.; Klebert, P. Loads and response on flexible conical and cylindrical fish cages: A numerical and experimental study based on full-scale values. *Ocean Eng.* **2020**, *216*, 107672. [[CrossRef](#)]
56. Wang, L.; Robertson, A.; Jonkman, J.; Kim, J.; Shen, Z.R.; Koop, A.; Borràs Nadal, A.; Shi, W.; Zeng, X.; Ransley, E.; et al. OC6 phase Ia: CFD simulations of the free-decay motion of the DeepCwind semisubmersible. *Energies* **2022**, *15*, 389. [[CrossRef](#)]
57. Ye, M.; Chen, H.; Koop, A. Verification and validation of CFD simulations of the NTNU BT1 wind turbine. *J. Wind. Eng. Ind. Aerodyn.* **2023**, *234*, 105336. [[CrossRef](#)]
58. Tran, T.T.; Kim, D. Fully coupled aero-hydrodynamic analysis of a semi-submersible FOWT using a dynamic fluid body interaction approach. *Renew. Energy* **2016**, *92*, 244–261. [[CrossRef](#)]

Disclaimer/Publisher’s Note: The statements, opinions and data contained in all publications are solely those of the individual author(s) and contributor(s) and not of MDPI and/or the editor(s). MDPI and/or the editor(s) disclaim responsibility for any injury to people or property resulting from any ideas, methods, instructions or products referred to in the content.